M2 MSIAM - Modeling seminar

Linnea Hallin, Éloi Navet, Maxime Renard & Nicolas Roblet

Under the direction of
Brigitte Bidegaray-Fesquet & Clément Jourdana

School year 2023-2024

Article studied:

A friendly review of Absorbing Boundary Conditions and perfectly matched layers for classical and relativistic quantum waves equations.

Author: X. Antoine, E. Lorin, and Q. Tang

Institut Elie Cartan de Lorraine, Université de Lorraine, UMR 7502, Inria Nancy-Grand Est;

Received October 2017

Key words: classical quantum waves; relativistic quantum waves; Schrödinger equation; Klein-Gordon equation; Dirac equation; Absorbing Boundary Conditions; perfectly matched layers; numerical schemes; simulation.

Contents

1 Introduction

1.1 Project context

This document was written as part of a modeling seminar organized by the MSIAM master's program. The aim is to carry out an initial research study in teams of 4. In order to carry out our research, we have been provided with a research paper as a support [1]. The aim is to understand and retrieve the results presented in this paper, and then to go deeper into the aspects that are of interest to us.

The project was produced by Linnea Hallin, Éloi Navet, Maxime Renard, and Nicolas Roblet under the supervision of Ms. Brigitte Bidegaray-Fesquet[1] and Mr. Clément Jourdana[1].

1.2 Presentation of the studied article

In the realm of numerical simulations, solving Partial Differential Equations (PDEs) necessitates working within a closed and bounded spatial domain. Given that wave propagation is a physical phenomenon extending beyond bounded domains, selecting appropriate boundary conditions becomes a pivotal concern. The aim is to construct artificial boundary conditions that effectively mimic the exact solution throughout the entire spatial domain.

In addressing this query, our primary resource will be the article [1], which delves into the topic of Transparent Boundary Conditions (TBCs), more precisely Absorbing Boundary Conditions (ABCs) and Perfectly Matched Layers (PMLs). On the one hand, ABCs consist in finding new equations, valid for space boundary points, that avoid getting reflections of the waves; reflections that would have no physical meaning as only due to the truncation of the domain for numerical simulation. This paradigm is presented on wave, diffusion and Schrödinger equations, so will we do. On the other hand, PMLs consist in introducing a specialized absorbing layer surrounding the computational domain. This layer is designed to dampen outgoing waves, mitigating the reflection issues encountered in traditional simulations with finite boundaries. The incorporation of complex-valued coefficients in the PML formulation allows for an effective absorption of waves as they approach the boundary. Essentially, PMLs extend the simulation domain into this absorbing layer, providing a solution to the challenges posed by unbounded wave propagation.

1.3 Overview of our study

The study is structured around a gradual progression of difficulty, consistent with the article [1] that serves as study support. The following is an overview of what we have achieved.

We began by simulating the wave equation, integrating classical boundary conditions such as Dirichlet and Neumann. Subsequently, we implemented the first TBCs introduced in the article, more precisely the ABCs. With the aim of broadening our field of study, we undertook an analysis of the diffusion equation. However, this exploration was only an intermediate step, as it was not the equation to which we devoted most of our attention. Once this phase was completed, we turned our attention to the Schrödinger equation. In a similar way, we started by implementing the classical boundary conditions, then added the ABCs. Once this was complete, we implemented the PMLs for this equation. To increase the flexibility of the simulation, we included the possibility of simulating the equation with a potential.

In parallel with the progress of the main study, we deliberately broadened our scope of investigation beyond the elements strictly addressed in the article. This approach was intended to enrich our analysis and explore subjects we value. Mainly, we preferred to take a rigorous look at the theoretical points addressed in the numerical study. This is part of our commitment to completeness, leaving as few theoretical grey areas as possible. With this in mind, we have chosen to focus on the theoretical aspects rather than rushing into the implementation of other equations such as the Dirac equation, the Klein-Gordon equation, or the two-dimensional Schrödinger equations. We prefer to understand the article's innovations in depth, rather than trying to implement them for various equations. However, this could prove to be a very interesting study, but it is not the path we have decided to take in the course of our study. In other words, we decided to carry out as complete a theoretical study as possible of all the important and innovative concepts discussed in the article, as well as their digital implementation.

[1] Univ. Grenoble Alpes, Grenoble INP

Therefore, this report is divided into two parts. A first, the main one, presenting the equations, the diagrams and their simulations and a second, the appendix, which contains the purely theoretical points (and also the diffusion equation at the end).

1.4 Notations

When dealing with schemes, it is important to have clear notations. For this purpose, we will consider a spatial uniform grid indexed by $j \in [\![0, J]\!]$, meaning having J sub-intervals and $J+1$ mesh points, and a uniform time grid indexed by $n \in \{0, \dots, N\}$. The corresponding notation for the approximation of an analytical solution ψ at space-time mesh points (j, n) will be ψ_j^n. The space (resp. time) step will be denoted Δx (resp. Δt). All of our schemes will make use of finite differences (FD) and we take the convention that for any j as defined before, and for any $0 \leq m \leq n, \psi_j^m$ is known, thus our schemes aim at finding ψ_j^{n+1}.

2 One-dimensional Wave Equation

2.1 Equation Discretization Scheme

Consider the one-dimensional wave equation with a constant speed in free space, for different boundary conditions. The governing equation is expressed as

$$\partial_{tt}\psi - c^2\partial_{xx}\psi = 0, \tag{1}$$

where $\psi : \mathbb{R}_x \times]0, T] \to \mathbb{R}$ represents the wave function and c is the wave velocity. It is crucial to note that, for a well-posed problem, the wave equation demands an initial condition for both ψ and its first-order time derivative.

To numerically solve this equation, a finite difference scheme is employed. Utilizing the Taylor-Lagrange formula, a centered second-order approximation for the second derivative of a function u with respect to space or time, given a small variation h, is obtained as follows:

$$u^{(2)}(x) = \frac{u(x+h) - 2u(x) + u(x-h)}{h^2} + \mathcal{O}(h^2).$$

Applying this continuous relation to the spatial and temporal mesh of the domain yields an approximation of equation (1):

$$\begin{aligned} \frac{\psi_j^{n+1} - 2\psi_j^n + \psi_j^{n-1}}{\Delta t^2} &= c^2 \frac{\psi_{j+1}^n - 2\psi_j^n + \psi_{j-1}^n}{\Delta x^2} \\ \Rightarrow \qquad \psi_j^{n+1} &= 2\psi_j^n - \psi_j^{n-1} + c^2 \frac{\Delta t^2}{\Delta x^2}(\psi_{j+1}^n - 2\psi_j^n + \psi_{j-1}^n). \end{aligned} \tag{2}$$

As demonstrated in appendix D.1, this scheme exhibits consistency of order 2 in both time and space and adheres to the Courant–Friedrichs–Lewy (CFL) condition given by $C := c\frac{\Delta t}{\Delta x} < 1$. It is important to highlight that no computation is required for time steps $n = 0$ and $n = 1$ since the initial value problem associated with this equation requires the function and its derivative at time 0.

While this scheme is applicable within the interior of the spatial domain, i.e., $j \in \{1, \dots, J-1\}$, specific boundary conditions must be specified for $j \in \{0, J\}$. The forthcoming discussion delves into boundary conditions and their implications.

Simulation parameters For all simulations in this section, the following set of parameters is adopted: $T = 0.5$, $\#T_{\text{mesh}} = 1000$, $\Omega = [-1, 2]$, $\#X_{\text{mesh}} = 500$, and $c = 6$. The initial condition comprises a sum of two Gaussians, illustrated in fig. 1. The first two time steps are initialized with the profile fig. 1.

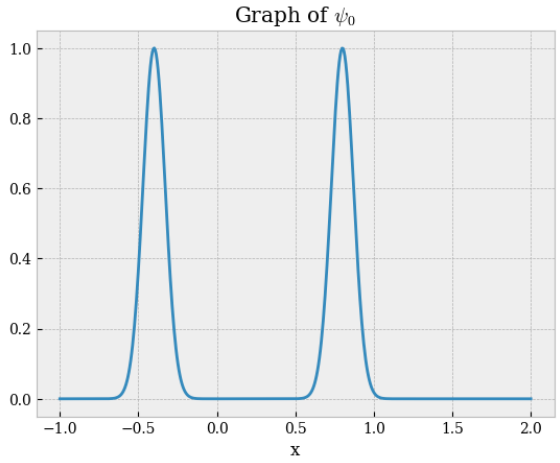

Figure 1: ψ_0 for the wave equation.

2.2 Classic Boundary Conditions

Dirichlet Boundary Condition

The Dirichlet boundary condition involves specifying the values of the wave at the boundaries of the computational domain. Mathematically, this is expressed as

$$\forall n \geq 0, \qquad \begin{cases} \psi_0^{n+1} = \alpha \\ \psi_J^{n+1} = \beta \end{cases} \qquad \text{with } (\alpha, \beta) \in \mathbb{R}^2.$$

Note it implies a compatibility relation for the time initialization, assuming ψ^0 and ψ^1 satisfy it. The simulation results in behaviour akin to a wave propagating along a string attached at both ends, as illustrated in fig. 2.

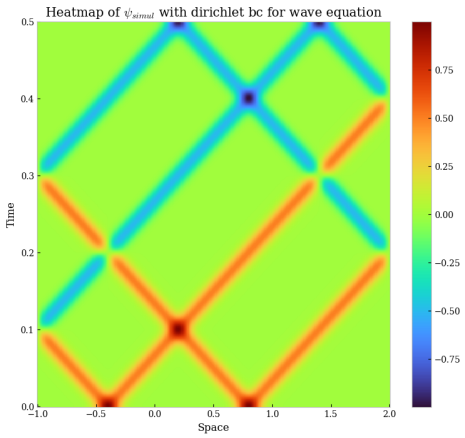

Figure 2: Simulation of (2) for Dirichlet boundary conditions with $\alpha = 0$ and $\beta = 0$.

Periodic Boundary Condition

The periodic boundary condition treats the boundaries of the computational domain as if they wrap around, creating a continuous, repeating space. This approach simulates an infinite and repetitive environment, where any object leaving the simulation through one boundary re-enters from the opposite boundary. To implement this, the numerical scheme is applied at each side of the domain, specifically at the boundary. The terms that do not exist on one side are replaced with the corresponding values from the opposite boundary. This exchange facilitates communication between the two sides, effectively wrapping the space around.

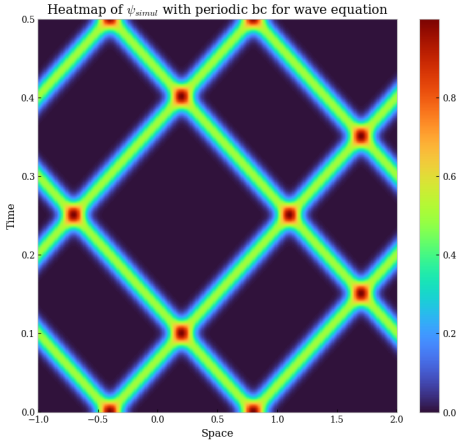

Figure 3: Simulation of (2) with periodic boundary conditions.

For this purpose, the scheme (2) is applied at points $j = 0$ and $j = J$, and then associated with $j : -1 \mapsto J$ (resp. $j : J + 1 \mapsto 0$) for the left (resp. right) boundary:

$$\forall n \geq 1, \quad \begin{cases} \psi_0^{n+1} = 2\psi_0^n - \psi_0^{n-1} + c^2 \dfrac{\Delta t^2}{\Delta x^2}(\psi_1^n - 2\psi_0^n + \psi_J^n) \\ \psi_J^{n+1} = 2\psi_J^n - \psi_J^{n-1} + c^2 \dfrac{\Delta t^2}{\Delta x^2}(\psi_0^n - 2\psi_J^n + \psi_{J-1}^n) \end{cases}$$

The plot in fig. 3 illustrates the time evolution (ordinate) of a wave propagating in space (abscissa), showcasing the expected behaviour of a wave in a wrapped space.

Neumann Boundary Condition

The Neumann boundary condition imposes a value on the normal derivative of the wave function, quantifying the quality of the reflected wave. For homogeneous Neumann conditions, the border is perfectly reflective as no portion of the wave penetrates the border.

Let α denote the desired value for $\partial_n \psi$ on the left border and β its value on the right border. Since the interior scheme is of order 2, the boundary scheme should also be of the same order to preserve the overall accuracy:

$$\begin{cases} \partial_n \psi|_0^{n+1} = \dfrac{1}{2\Delta x}\left(3\psi_0^{n+1} - 4\psi_1^{n+1} + \psi_2^{n+1}\right) \\ \partial_n \psi|_J^{n+1} = \dfrac{1}{2\Delta x}\left(\psi_{J-2}^{n+1} - 4\psi_{J-1}^{n+1} + 3\psi_J^{n+1}\right) \end{cases}$$

These decentered schemes lead to the following second-order explicit boundary schemes:

$$\begin{cases} \psi_0^{n+1} = \dfrac{1}{3}\left[2\alpha\Delta x + 4\psi_1^{n+1} - \psi_2^{n+1}\right] \\ \psi_J^{n+1} = \dfrac{1}{3}\left[2\beta\Delta x + 4\psi_{J-1}^{n+1} - \psi_{J-2}^{n+1}\right] \end{cases}$$

The simulation effectively demonstrates how the boundary functions like a mirror in the case of homogeneous Neumann conditions, resulting in a perfect reflection, as shown in fig. 4. Unlike Dirichlet boundary conditions, no sign inversion occurs during the reflection of the wave.

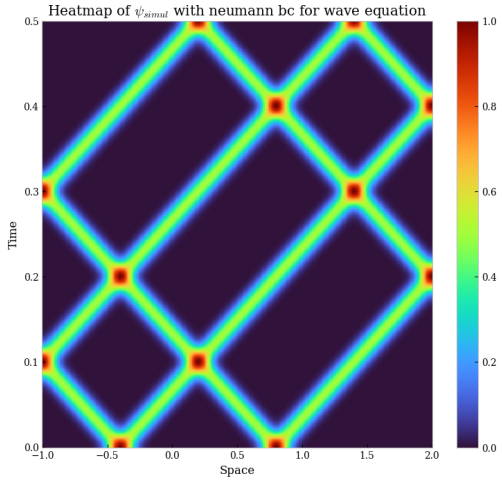

Figure 4: Simulation of (2) with Neumann boundary conditions ($\alpha = 0$ and $\beta = 0$).

2.3 Adding a Source Term

For this part, a source term Q is introduced to the wave equation, with $Q \geq 0$. Although Q could theoretically be non-punctual, if it does not decay over time, the solution to the wave equation becomes unbounded. The non-homogeneous wave equation is given by:

$$\partial_{tt}\psi - c^2\partial_{xx}\psi = c^2 Q. \tag{3}$$

To incorporate Q into the interior scheme (2), $2\Delta x Q$ is added to the right-hand side. Energy analysis on this non-homogeneous version is performed in appendix C.1, and equation (67) provides the evolution of the total energy E inside the domain as:

$$E(t) = E(0) + \left(\frac{c^2}{2}\int_\Omega Q(x,t)\psi(x,t)dx\right)(t) - \left(\frac{c^2}{2}\int_\Omega Q(x,t)\psi(x,t)dx\right)(t=0). \tag{4}$$

This expression is consistent, as when $Q \equiv 0$, total energy is preserved over time, while if $Q > 0$, energy increases over time. In the following, we have equated physical energy with the L^2 norm only in the hope of seeing it increase. We can note that although we haven't shown it, in previous simulations it was preserved.

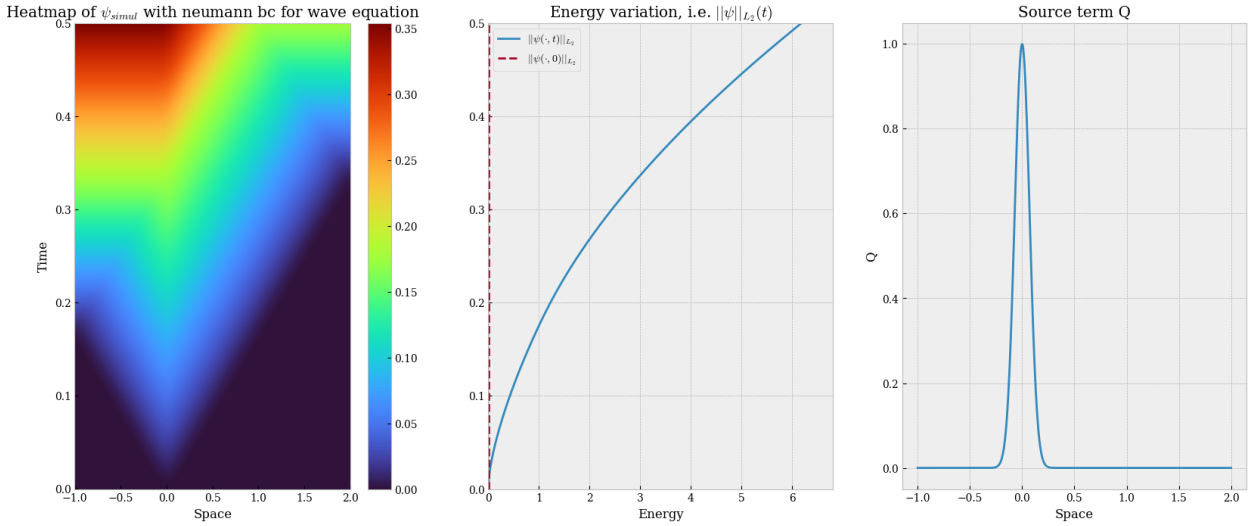

Figure 5: Simulation of (3) with null initial conditions, using Neumann boundary condition $(0,0)$ and $Q(x) = e^{-100x^2}$.

For a constant source term over time, fig. 5 illustrates how energy accumulates in the domain. The homogeneous Neumann boundary condition reflects all waves, thus energy, into the domain. Note that the simulation was initialized without a wave.

2.4 Absorbing Boundary Condition

In this section, Absorbing Boundary Conditions are introduced to the wave equation, as proven in appendix A.1. This implementation aims to provide an understanding of their origin and serves as a foundation for implementing them in the Schrödinger equation. The simulation considers the following system of equations:

$$\begin{cases} \partial_{tt}\psi - c^2\partial_{xx}\psi = 0 & \text{in} \quad \Omega \times (0,T), \\ \psi(\cdot,0) = \psi_0, \quad \partial_t\psi(\cdot,0) = \psi_{t,0} & \text{on} \quad \Omega, \\ \partial_n\psi(x,t) + \frac{1}{c}\partial_t\psi(x,t) = 0 & \text{on} \quad \partial\Omega \times [0,T]. \end{cases}$$

The goal is to find a discrete approximation of $\partial_n\psi + \frac{1}{c}\partial_t\psi = 0$ while preserving second-order accuracy. One can't use the scheme (2) since this will make non-existing mesh point appear, which is not possible in this case as this will impose another boundary condition. To solve this issue, the space derivative in the normal

derivative is approximated using a second-order forward scheme for the left boundary and a second-order backward scheme for the right boundary:

$$\begin{cases} \partial_n \psi|_0^{n+1} = \dfrac{1}{2\Delta x}\left(3\psi_0^{n+1} - 4\psi_1^{n+1} + \psi_2^{n+1}\right) \\ \partial_n \psi|_J^{n+1} = \dfrac{1}{2\Delta x}\left(\psi_{J-2}^{n+1} - 4\psi_{J-1}^{n+1} + 3\psi_J^{n+1}\right) \end{cases}$$

For the time derivative, the usual second-order centered approximation used before is retained, as no particular issue arises:

$$\partial_t \psi|_j^{n+1} = \frac{\psi_j^{n+1} - \psi_j^{n-1}}{2\Delta t}.$$

When combined with the normal derivative schemes, the two following explicit relations are obtained:

$$\begin{cases} \psi_0^{n+1} = \dfrac{1}{\Delta x + 3c\Delta t}\left[4c\Delta t.\psi_1^{n+1} - c\Delta t.\psi_2^{n+1} + \Delta x.\psi_0^{n-1}\right] \\ \psi_J^{n+1} = \dfrac{1}{\Delta x + 3c\Delta t}\left[4c\Delta t.\psi_{J-1}^{n+1} - c\Delta t.\psi_{J-2}^{n+1} + \Delta x.\psi_J^{n-1}\right] \end{cases} \tag{5}$$

It is crucial to note that this Transparent Boundary Condition scheme relies on the knowledge of ψ^{n+1} on the interior of the domain. In essence, this boundary condition necessitates applying the scheme on the interior of the domain (2) first and then propagating the information to the boundary. Thus, it remains an explicit scheme, even though the relations are written at time step $n+1$.

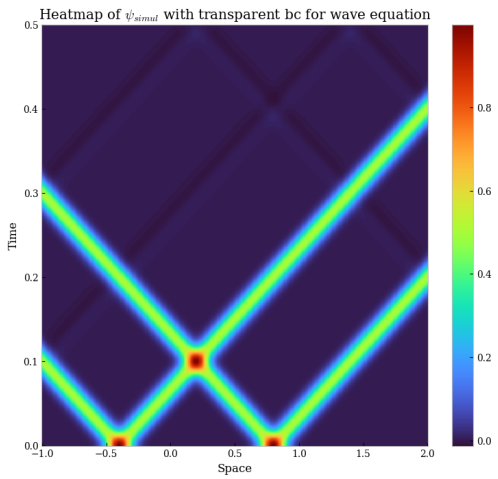

Figure 6: Simulation of (2) with Absorbing Boundary Conditions.

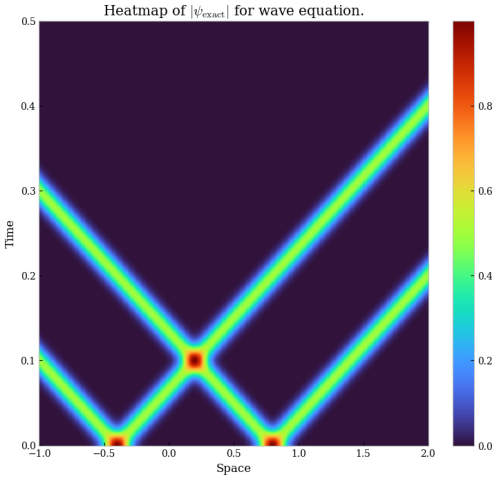

Figure 7: Exact solution (54).

2.5 Study of the Complete Initial Value Problem

Now, let us investigate the initial value problem for the wave equation with a non-zero initial time derivative:

$$\begin{cases} \partial_{tt}\psi - c^2\partial_{xx}\psi = 0 & \text{in} \quad \mathbb{R}\times(0,T), \\ \psi(\cdot,0) = \psi_0, \quad \partial_t\psi(\cdot,0) = \psi_{t,0} & \text{on} \quad \mathbb{R}. \end{cases} \tag{6}$$

As mentioned in the introduction for scheme (2), the initial wave and its derivative must be provided at time $n = 0$ for the wave equation to be well-posed. To be precise, ψ_0 and $\psi_{0,t}$ must be supplied for a well-posed problem. Therefore, for the simulation, the following equation is implemented:

$$\begin{aligned} \forall j \in [\![0, J]\!], \qquad \psi_j^1 &= \psi_0(x_j) + \psi_{t,0}(x_j)\Delta_t \\ &= \psi_j^0 + \psi_{t,0}(x_j)\Delta_t. \end{aligned} \tag{7}$$

Previously, one always considered that the initial time derivative was zero. To test this implementation, one will focus on the case of a right-going wave only.

Right-Going Transport Only

To test the simulation model, we consider initial conditions such that the solution is composed of right-going waves only, i.e.,

$$\forall (x,t) \in \mathbb{R} \times (0,+\infty), \qquad \psi(x,t) = \psi_0(x-ct).$$

Starting with d'Alembert's formula (54), we have:

$$\begin{aligned}\forall (x,t) \in \mathbb{R} \times (0,+\infty), \qquad \psi(x,t) &= \frac{1}{2}[\psi_0(x+ct) + \psi_0(x-ct)] + \frac{1}{2c}\int_{x-ct}^{x+ct} \psi_{t,0}(y)\,dy \\ &= \frac{1}{2}\psi_0(x+ct) + \frac{1}{2c}\int_0^{x+ct} \psi_{t,0}(y)\,dy + \frac{1}{2}\psi_0(x-ct) + \frac{1}{2c}\int_{x-ct}^{0} \psi_{t,0}(y)\,dy,\end{aligned}$$

which is the analytical solution of the initial value problem. We want initial values such that

$$\frac{1}{2}\psi_0(x+ct) + \frac{1}{2c}\int_0^{x+ct} \psi_{t,0}(y)\,dy = 0.$$

Differentiating the above equation with respect to time, we get:

$$\frac{c}{2}\psi_0'(x+ct) + \frac{1}{2}\psi_{t,0}(x+ct) = 0 \qquad \Rightarrow \qquad \psi_{t,0}(x) = -c\psi_0'(x). \tag{8}$$

Then,

$$\begin{aligned}\forall (x,t) \in \mathbb{R} \times (0,+\infty), \qquad \psi(x,t) &= \frac{1}{2}\psi_0(x-ct) - \frac{1}{2}\int_{x-ct}^{0} \psi_0'(y)\,dy \\ &= \psi_0(x-ct).\end{aligned}$$

A simulation according to (7) and (8) is shown in fig. 8. This result aligns with the expected behavior of the constructed solution. However, some residuals remain, so for a more detailed analysis we will examine the error carried by the simulation.

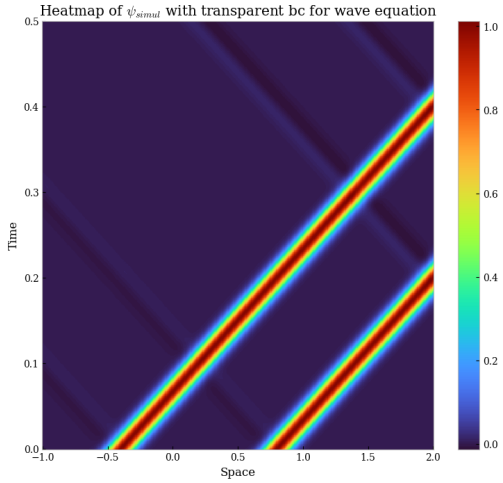

Figure 8: Experiment with waves propagating exclusively to the right, consistent with (7) and (8).

2.6 Study of the Error

In the following development, the focus is exclusively on the Transparent Boundary Condition, as it is the primary concern of this article.

2.6.1 Error with Respect to the Exact Solution

Throughout the study, various error analyses are conducted. To eliminate the order of magnitude of the simulated system, the following relative error (with respect to the exact solution) is considered:

$$\forall t, \qquad e_r(t) = \frac{\max\limits_{x}(|\psi_{\text{sim}}(x,t) - \psi_{\text{ex}}(x,t)|)}{\max\limits_{x,t'}(|\psi_{\text{ex}}(x,t')|)}. \tag{9}$$

Necessarily, the exact solution needs to be implemented. In this case, as proven in appendix B.1, the exact solution of the initial value problem (6) is the d'Alembert's formula (54):

$$\forall (x,t) \in \mathbb{R} \times (0,+\infty), \qquad \psi(x,t) = \frac{1}{2}[\psi_0(x+ct) + \psi_0(x-ct)] + \frac{1}{2c}\int_{x-ct}^{x+ct} \psi_{t,0}(y)\ \mathrm{d}y.$$

The main challenge in implementing this is calculating the integral. As it is necessary to compute $\#T_{\text{mesh}} \times \#X_{\text{mesh}}$ points, a fast method is used. Integrals are approximated using the composite trapezoidal rule. The full development of the committed error can be found in section 2.4, leading to the result shown in fig. 9.

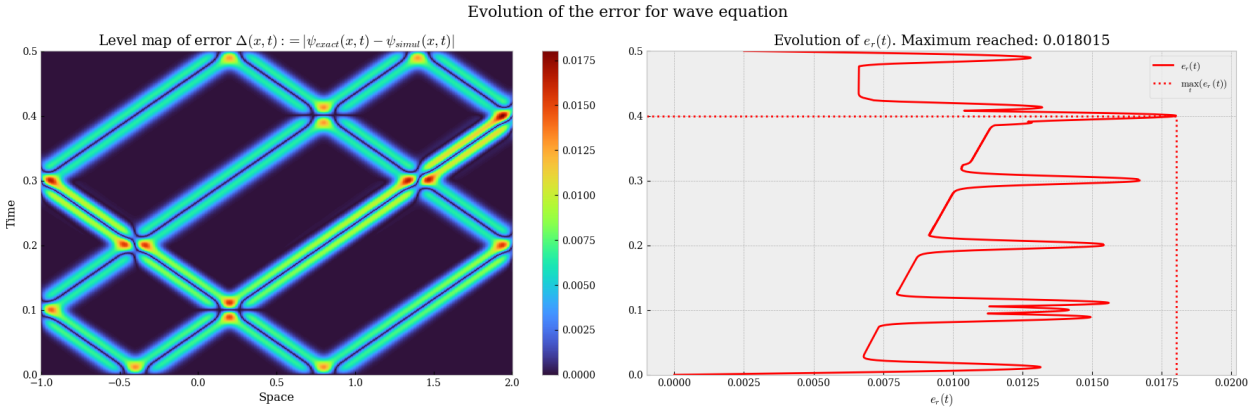

Figure 9: Exact error of the wave equation (1) simulation using ABCs.

The most important observation is that the order of magnitude of edge absorption is approximately 99%, meaning that the relative error e_r is approximately 1%. Moreover, the error committed during the simulation is of the same order of magnitude before and after the partial bounces at the edge of the simulation, at least for our measure. Therefore, it is interesting to note that our boundary condition schemes do not generate a significant error compared to our discretization of the wave equation. For a more detailed study of the consequence of ABC, it might be interesting to reduce the order of the wave equation scheme.

Another way to overcome the error of our equation discretization scheme, to concentrate only on the influence of the choice of our boundary conditions scheme, is presented in the following section.

2.6.2 Isolating Reflections

Given the known performance derived from the exact error analysis of ABCs for the wave equation, where they remain unaffected by schematic errors, the process of reflection isolation may not have immediate relevance. However, to exemplify the principle of isolating reflections, which proves essential for the Schrödinger equation, we leverage the simplicity inherent in the wave equation.

The preceding analysis provided insights into the absorption performance. Nonetheless, as will be demonstrated in the context of the Schrödinger equation, such a study can become intricate.

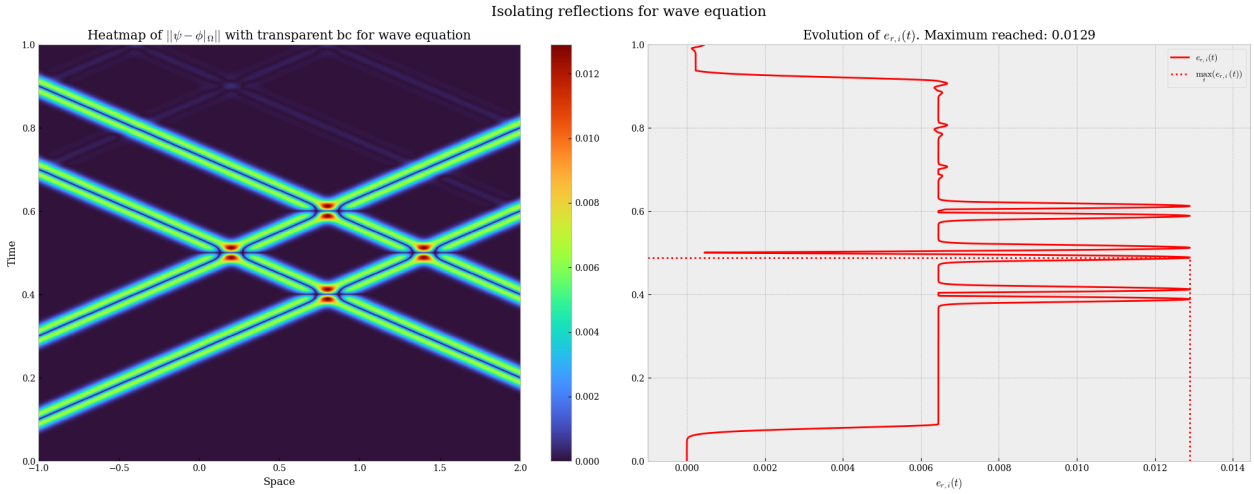

Figure 10: Isolated reflections of the wave equation (1) using ABCs.

The concept of isolating reflections aims to liberate the analysis from the constraints of the exact solution, focusing solely on the influence of the boundary condition on the computation. The procedure entails isolating the reflections observed in fig. 6 and quantifying their order of magnitude. For this purpose, the same simulation will be run on a larger domain, providing a result ϕ. To isolate reflections, this larger domain is defined by extending both sides of Ω by a segment of the same size as Ω, so that reflections do not have enough time to get back to Ω. For example, if ψ is computed over $[-1, 2]$ with 500 points in space, then ϕ is computed on $[-4, 5]$ with $3 \times 500 - 2 = 1498$ points in space. Then, reflections are isolated in the function $\psi - \phi|_\Omega$.

To evaluate their orders of magnitude, the following measurement, analogous to the one considered in the previous part, is used:

$$\forall t, \qquad e_{r,i}(t) = \frac{\max\limits_{x \in \Omega}(|\psi(x,t) - \phi|_\Omega(x,t)|)}{\max\limits_{t', x \in \Omega}(|\psi(x,t')|)}. \tag{10}$$

The results are presented in fig. 10. One observes that the order of magnitude of the relative error committed by the ABCs is around 1%, which is consistent with our previous results, since the errors considered have the same semantics but for slightly "different" objects.

3 Schrödinger Equation

3.1 Equation Discretization Scheme

The subject of this part is the Schrödinger equation, as presented in [1] and expressed as:

$$\begin{cases} \partial_t \psi^{\text{int}} - i\partial_{xx}\psi^{\text{int}} = i\mathbb{V}\psi^{\text{int}}, & (x,t) \in \Omega_T, \\ \psi^{\text{int}}(x,0) = \psi_0(x), & x \in \Omega. \end{cases} \tag{11}$$

We will denote ψ^{int} as ψ for readability. $\mathbb{V}$ is a space-time-dependent potential, potentially non-linear depending on ψ. We will denote V the part of the potential depending only on space and time, and f as the non-linear part, i.e., $\mathbb{V}(x,t) = V(x,t) + f(\psi)(x,t)$. Boundary conditions must be provided for well-posedness. Note that **for this section** we can draw an analogy with the previous calculations by choosing **c=i**, and Crank-Nicolson scheme is used on (11), giving:

$$\frac{\psi_j^{n+1} - \psi_j^n}{\Delta t} = \frac{c}{2(\Delta x)^2}\left[\left(\psi_{j+1}^{n+1} - 2\psi_j^{n+1} + \psi_{j-1}^{n+1}\right) + \left(\psi_{j+1}^{n} - 2\psi_j^{n} + \psi_{j-1}^{n}\right)\right] + \frac{c}{2}V_j^{n+1}\left(\psi_j^{n+1} + \psi_j^n\right). \tag{12}$$

As shown in the appendix D.2, this scheme is consistent of order 1 in time, order 2 in space, with only diffusion error, and it is unconditionally stable.As this is an implicit scheme, it can be solved using linear algebra. The focus is on the inside of the domain Ω. Denote $\psi^{n+1} = \left(\psi_0^{n+1}, \dots, \psi_J^{n+1}\right)$ as the vector to be computed for each time step. Then the main equation of (11) can be expressed in terms of ψ^{n+1} as:

$$A^{n+1}\psi^{n+1} = B^{n+1}\psi^n + S^{n+1}, \tag{13}$$

where the only unknown is ψ^{n+1}, and matrices A and B are defined as:

$$A^{n+1} = \begin{pmatrix} \cdot & \cdot & \cdot & \dots & \cdot & \cdot & \cdot \\ -\frac{C}{2} & 1+C-\tilde{V_1^{n+1}} & -\frac{C}{2} & 0 & \dots & \dots & \vdots \\ 0 & \ddots & \ddots & \ddots & \ddots & \ddots & \vdots \\ \vdots & \ddots & \ddots & \ddots & \ddots & \ddots & \vdots \\ \vdots & \vdots & \ddots & \ddots & \ddots & \ddots & 0 \\ \vdots & \vdots & \dots & 0 & -\frac{C}{2} & 1+C-\tilde{V_{J-1}^{n+1}} & -\frac{C}{2} \\ \cdot & \cdot & \cdot & \dots & \cdot & \cdot & \cdot \end{pmatrix} \quad B^{n+1} = \begin{pmatrix} \cdot & \cdot & \cdot & \dots & \cdot & \cdot & \cdot \\ \frac{C}{2} & 1-C+\tilde{V_1^{n+1}} & \frac{C}{2} & 0 & \dots & \dots & \vdots \\ 0 & \ddots & \ddots & \ddots & \ddots & \ddots & \vdots \\ \vdots & \ddots & \ddots & \ddots & \ddots & \ddots & \vdots \\ \vdots & \vdots & \ddots & \ddots & \ddots & \ddots & 0 \\ \vdots & \vdots & \dots & 0 & \frac{C}{2} & 1-C+\tilde{V_{J-1}^{n+1}} & \frac{C}{2} \\ \cdot & \cdot & \cdot & \dots & \cdot & \cdot & \cdot \end{pmatrix} \tag{14}$$

where $C = c\frac{\Delta t}{(\Delta x)^2}$ is the Courant–Friedrichs–Lewy (CFL) number, and $\tilde{V_j^n} = \frac{i}{2}V_j^n$. S^{n+1} is defined as a column vector helpful to introduce boundary conditions such as Dirichlet. The first and last rows of the matrices A^{n+1} and B^{n+1} are left empty to allow for the implementation of spatial boundary conditions. Now, let us discuss the simulation parameters. For all the simulations in this section, we consider the following parameters: $T = 2$, $\#T_{\text{mesh}} = 501$, $\Omega = [-10, 10]$, $\#X_{\text{mesh}} = 501$, and

$$\forall x \in \mathbb{R}, \quad \psi_0(x) = 2\,\text{sech}(\sqrt{2}x)e^{i\frac{15}{2}x}.$$

These values are not exactly the same as in the article [1]. For the purpose of result comparison, this difference is of little importance since they do not present an error study. These values are chosen to maintain a reasonable complexity and to have an interesting error study. Note that for each simulation, the temporal evolution of its L_2 energy is added. The aim is to check that the simulation preserves the conservation property and to roughly evaluate the energy loss during the encounter between the wave and the boundary. The conservation of the L_2 norm for the Schrödinger equation is shown in appendix C.2.

3.2 Classic Boundary Conditions

Dirichlet Boundary Conditions

For the homogeneous Dirichlet boundary condition, we prescribe the values of the unknown function on the boundary, denoted as α on the left side and β on the right side:

$$\forall n \geq 0, \qquad \begin{cases} \psi_0^{n+1} = \alpha, \\ \psi_r^{n+1} = \beta, \end{cases} \qquad \text{with } (\alpha, \beta) \in \mathbb{R}^2.$$

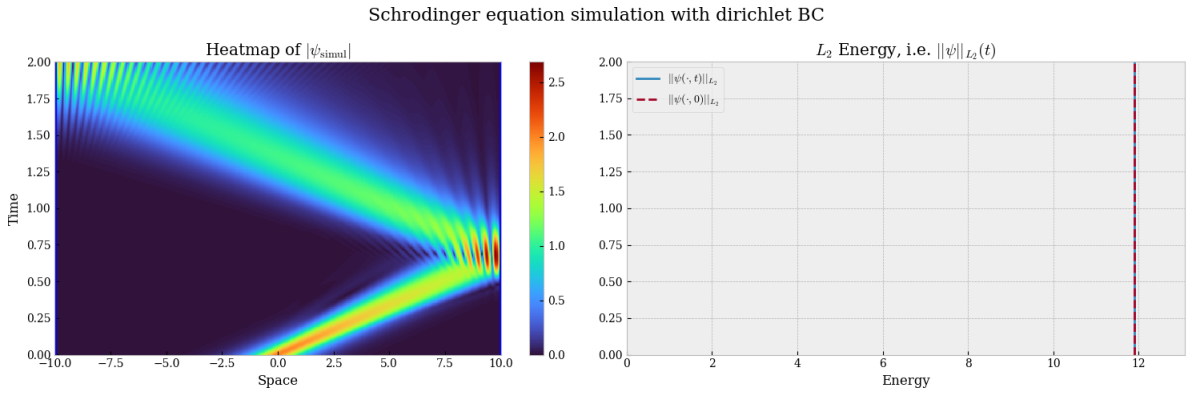

Figure 11: Simulation of (11) for homogeneous Dirichlet boundary condition.

This leads to $A^{n+1}_{0,0} = A^{n+1}_{J,J} = 1$ and 0 on the other coefficients of the first and last lines. For B^{n+1}, the first and last lines are null. Finally, $S^{n+1}_{0,0} = \alpha$ and $S^{n+1}_{J,J} = \beta$. We observe that the conservation of the energy and the non-dispersion of the boundary conditions aligns with expectations.

Neumann Boundary Conditions

Recall that Neumann condition describes the reflective property of the boundary, i.e., how much of the wave can go through it. It also induces a compatibility relation with the initialization of the wave. In fact, if the initial profile of the wave does not satisfy the boundary condition, some relaxation could occur. For the homogeneous Neumann boundary condition, which describes the reflective property of the boundary, we use second-order decentered schemes for the normal derivatives:

$$\begin{cases} \partial_{\mathbf{n}}\psi|^n_0 &= \frac{1}{2\Delta x}\left(3\psi^n_0 - 4\psi^n_1 + \psi^n_2\right) = \alpha \\ \partial_{\mathbf{n}}\psi|^n_J &= \frac{1}{2\Delta x}\left(\psi^n_{J-2} - 4\psi^n_{J-1} + 3\psi^n_J\right) = \beta. \end{cases} \tag{15}$$

Completing the corresponding coefficients in the matrices is then simple:

$$\begin{cases} A^{n+1}_{0,\cdot} = \dfrac{1}{2\Delta x}\left(3, -4, 1, 0 \ldots, 0\right) \\ A^{n+1}_{J,\cdot} = \dfrac{1}{2\Delta x}\left(0, \ldots, 0, 1, -4, 3\right) \end{cases} \text{ and } \begin{cases} B^{n+1}_{0,\cdot} = (0, \ldots, 0) \\ B^{n+1}_{J,\cdot} = (0, \ldots, 0) \end{cases} \text{ and } (S^{n+1})^T = (\alpha, 0, \ldots, 0, \beta)\,.$$

The results show a reflective boundary, with the wave touching it, unlike the case of homogeneous Dirichlet condition. The conservation of our digital system is once again evident. Imposing that the normal derivative has value α on the left side and β on the right side leads to very similar results as Dirichlet in the case of homogeneous Neumann condition, i.e., a perfectly reflective boundary. The results are presented in fig. 12.

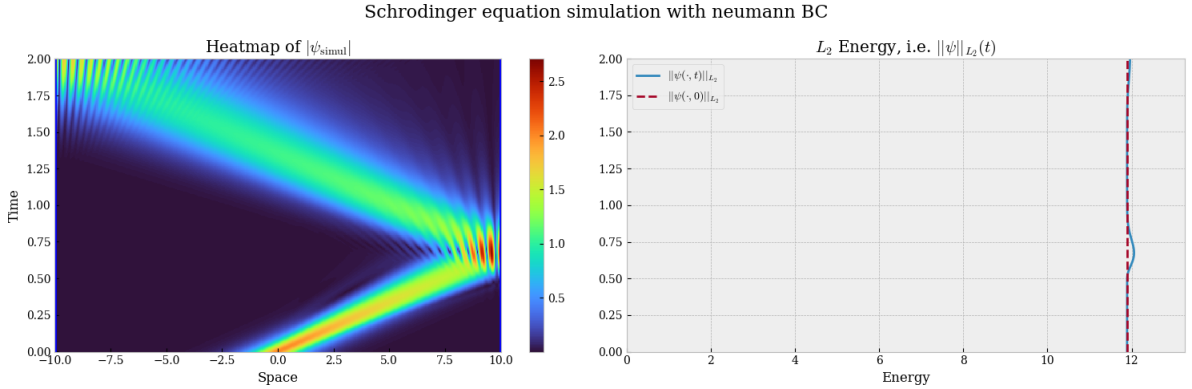

Figure 12: Simulation of (11) for homogeneous Neumann boundary condition.

It is important to mention that the wave touches the boundary, which is not the case for homogeneous Dirichlet conditions. Moreover, we are once again noting the conservation of our digital system.

3.3 Absorbing Boundary Condition

As discussed in the article [1] and proven in appendix A.2, the Transparent Boundary Condition for the homogeneous Schrödinger equation, i.e. with $\mathbb{V} \equiv 0$, is given by:

$$\partial_{\mathbf{n}}\psi^{\text{int}} + e^{-i\pi/4}\partial_t^{1/2}\psi^{\text{int}} = 0, \quad (x,t) \in \Sigma_T. \tag{16}$$

The spatial normal derivative on the boundaries at a given time n can be approximated by a second-order scheme:

$$\begin{cases} \partial_{\mathbf{n}}\psi|_0^n &= \frac{1}{2\Delta x}\left(3\psi_0^n - 4\psi_1^n + \psi_2^n\right), \\ \partial_{\mathbf{n}}\psi|_J^n &= \frac{1}{2\Delta x}\left(\psi_{J-2}^n - 4\psi_{J-1}^n + 3\psi_J^n\right). \end{cases} \tag{17}$$

For the Caputo derivative, the approximation used in the article is given by:

$$\partial_t^{\frac{1}{2}}\psi(t^n) \approx \sqrt{\frac{2}{\Delta t}}\sum_{k=0}^{n}\beta_k\psi^{n-k} \text{ where } \beta_k = (-1)^k\alpha_k, \tag{18}$$

where the formula for α_k was found in [2] and is given by

$$\alpha_k = \begin{cases} 1 & \text{if } k = 0 \text{ or } 1, \\ \gamma_k + \gamma_{k-1} & \text{else,} \end{cases} \quad \text{with} \quad \gamma_k = \begin{cases} 1 & \text{if } k = 0, \\ 0 & \text{if } k = 2p+1, \\ \prod_{j=1}^{p}\frac{2j-1}{2j} = \frac{2p-1}{2p}\gamma_{2(p-1)} & \text{if } k = 2p. \end{cases} \tag{19}$$

A scheme for the Transparent Boundary Condition, which is of second order in space, can be derived using (17) and (18). For readability, we denote $g = e^{-i\frac{\pi}{4}}\Delta x\sqrt{\frac{2}{\Delta t}}$.

- On the left:

$$\begin{aligned} &\frac{1}{2\Delta x}\left(3\psi_0^{n+1} - 4\psi_1^{n+1} + \psi_2^{n+1}\right) + e^{-i\frac{\pi}{4}}\sqrt{\frac{2}{\Delta t}}\sum_{k=0}^{n+1}\beta_k\psi_0^{n+1-k} = 0 \\ &\iff \underbrace{\left(\frac{3}{2} + g\beta_0\right)}_{=A_{0,0}}\psi_0^{n+1} + \underbrace{(-2)}_{=A_{0,1}}\psi_1^{n+1} + \underbrace{\frac{1}{2}}_{=A_{0,2}}\psi_2^{n+1} = \underbrace{-g\beta_1}_{=B_{0,0}}\psi_0^n + \underbrace{\left(-g\sum_{k=2}^{n+1}\beta_k\psi_0^{n+1-k}\right)}_{=S_0}. \end{aligned} \tag{20}$$

- On the right :

$$\begin{aligned} &\frac{1}{2\Delta x}\left(3\psi_J^{n+1} - 4\psi_{J-1}^{n+1} + \psi_{J-2}^{n+1}\right) + e^{-i\frac{\pi}{4}}\sqrt{\frac{2}{\Delta t}}\sum_{k=0}^{n+1}\beta_k\psi_0^{n+1-k} = 0 \\ &\iff \underbrace{\left(\frac{3}{2} + g\beta_0\right)}_{=A_{J,J}}\psi_J^{n+1} + \underbrace{(-2)}_{=A_{J,J-1}}\psi_{J-1}^{n+1} + \underbrace{\frac{1}{2}}_{=A_{J,J-2}}\psi_{J-2}^{n+1} = \underbrace{-g\beta_1}_{=B_{J,J}}\psi_0^n + \underbrace{\left(-g\sum_{k=2}^{n+1}\beta_k\psi_J^{n+1-k}\right)}_{=S_J}. \end{aligned} \tag{21}$$

For numerical approximation, schemes (20) and (21) coefficients for matrices A and B and vector S can be plugged into (14) to be able to use a linear solver for the transparent boundary Schrödinger problem. It is important to note that both boundary schemes have been multiplied by Δx to improve the condition number of A and B. Without this trick, $\text{Cond}(A) = 5532$, whereas now we have $\text{Cond}(A) = 5023$. This is not a major difference, but it is still significant for stable approximations. The implementation yields the results shown in fig. 13.

Some small unwanted reflections are observed, potentially due to the Crank-Nicolson scheme or the non-linearity used in the article. Additionally, the conservation of energy before meeting the boundary and significant dissipation at the boundary are evident. However, there are propagating residues, and a study in section 3.6 is dedicated to them.

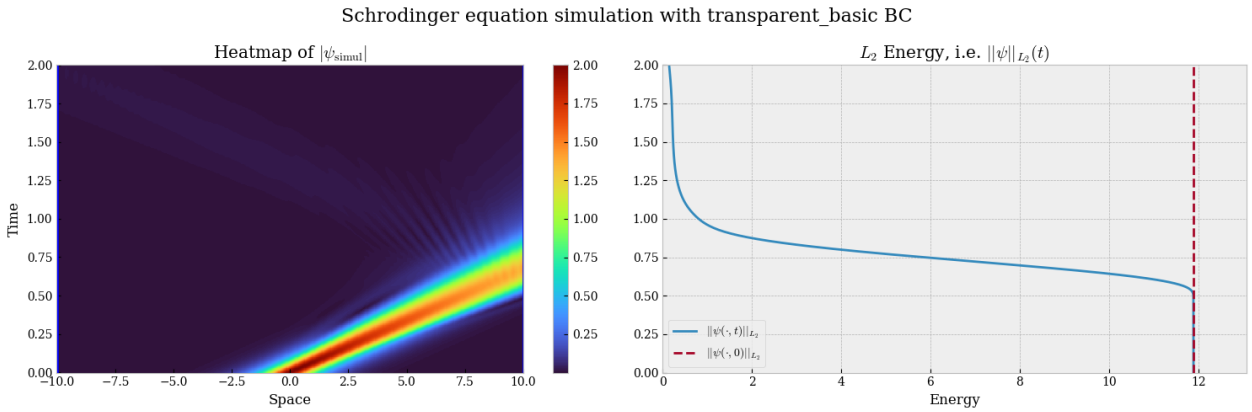

Figure 13: Simulation of (11) with Absorbing Boundary Condition.

3.4 Adding a Potential

As the Schrödinger equation can include an additional term in the form of a potential, which is used in the presentation of the results in the article, we chose to add this possibility to the code. We focused on a potential that does not introduce non-linearity, i.e., $\mathbb{V}(x,t) = V(x,t)$, as it is already quite some work to derive the corresponding schemes, even if the results of the article do include non-linear potential.

3.4.1 Continuous Framework

The corresponding Transparent Boundary Condition can be approximated using pseudodifferential operators theory and symbolical calculus, leading to, for example, a fourth-order version of the TBC presented in [1]:

$$\partial_n\psi + e^{-i\frac{\pi}{4}}e^{i\mathcal{V}}\partial_t^{1/2}\left(e^{-i\mathcal{V}}\psi\right) + i\text{sg}(\partial_n V)\frac{\sqrt{|\partial_n V|}}{2}e^{i\mathcal{V}}\text{I}_t\left(\frac{\sqrt{|\partial_n V|}}{2}e^{-i\mathcal{V}}\psi\right) = 0, \tag{22}$$

where:

- ∂_n denotes the normal derivative operator;
- sg is the sign function;
- $\partial_t^{1/2}$ is the Caputo fractional derivative operator;
- $\mathcal{V} = \text{I}_t V$;
- $\text{I}_t = \int_0^t$, integral over time 0 to t operator.

Some remarks on the arguments of all those terms are useful, which is not explicit with formulation (22).

3.4.2 From Continuous to Discrete Expression

Potential-Linked Terms

The potential V is a function of space and time, and the normal derivative $\partial_n V$ also depends on space and time, even if it can only be evaluated on the space boundary. The equality $\mathcal{V} = \text{I}_t V$ could also be written as $\mathcal{V}(x,t) = \text{I}_t(V(x,\cdot))$ where $\cdot$ denotes that the variable is integrated. As V is given data, its integral over time and normal derivatives can be computed before running any simulation. We will use the notation

$$\mathcal{V}_j^n := \mathcal{V}(j\Delta x, n\Delta t) = \int_0^{n\Delta t} V(j\Delta x, \tau)d\tau.$$

Quadrature Formulas

The boundary formula contains two integrals, Caputo fractional derivative, and I_t, which means methods to approximate these have to be chosen. For the Caputo fractional derivative we use the same one as for the homogeneous Transparent Boundary Condition. However, for I_t, we chose to start with a trapezoid method as it is easy to implement and of order 1, in contrast to rectangle methods that are of order 0. Recall that for a segment $[a, b]$ uniformly split into N intervals $([a_k, a_{k+1}])_{k\in\{0,\dots,N\}}$ of length δx, and over which a function h is defined, the approximation of the integral of h over this segment by the method of trapezoid is given by:

$$\int_a^b h(x)dx \approx \sum_{k=0}^{N} \frac{h(a_k)+h(a_{k+1})}{2}\delta x \approx \frac{\delta x}{2}\left(h_0 + h_{N+1}\right) + \delta x \sum_{k=1}^{N} h_k.$$

Note that in the case of a sequence of approximations of h at each interval boundary point a_k, we could replace $h(a_k)$ by its approximation h_k, which we will do when writing the scheme for (22).

3.4.3 The Boundary Scheme

Noting that for the normal derivatives, the same approximation formulas as provided in (17) are used both for $\mathcal{V}$ and ψ, we get the following scheme on the **left** boundary:

$$\begin{aligned}
&\frac{1}{2\Delta x}\left(3\psi_0^{n+1} - 4\psi_1^{n+1} + \psi_2^{n+1}\right) + e^{-i\frac{\pi}{4}} e^{i\mathcal{V}_0^{n+1}} \sqrt{\frac{2}{\Delta t}} \sum_{k=0}^{n+1} \left(\beta_k \psi_0^{n+1-k} e^{-i\mathcal{V}_0^{n+1-k}}\right) \\
&+ i\mathrm{sg}(\partial_n V|_0^{n+1}) \frac{\sqrt{\left|\partial_n V|_0^{n+1}\right|}}{2} e^{i\mathcal{V}_0^{n+1}} \left[\frac{\Delta t}{2}\left(\frac{\sqrt{\left|\partial_n V|_0^{0}\right|}}{2} e^{-i\mathcal{V}_0^{0}}\psi_0^0 + \frac{\sqrt{\left|\partial_n V|_0^{n+1}\right|}}{2} e^{-i\mathcal{V}_0^{n+1}}\psi_0^{n+1}\right)\right. \\
&\left. + \Delta t \sum_{k=1}^{n}\left(\frac{\sqrt{\left|\partial_n V|_0^{k}\right|}}{2} e^{-i\mathcal{V}_0^{k}}\psi_0^k\right)\right] = 0.
\end{aligned}$$

To get coefficients to inject into matrices A^{n+1}, B^{n+1} and S^{n+1}, one can split factors in front of ψ_j^{n+1}, ψ_j^n, and ψ_j^k for $k \le n-1$, and multiply the equation by Δx. We use again the notation $g = e^{-i\frac{\pi}{4}}\Delta x\sqrt{\frac{2}{\Delta t}}$ for readability purposes, leading to:

$$\begin{aligned}
&\underbrace{\left(\frac{3}{2} + g e^{i\mathcal{V}_0^{n+1}}\beta_0 e^{-i\mathcal{V}_0^{n+1}} + i\Delta x \mathrm{sg}(\partial_n V|_0^{n+1})\frac{\Delta t}{2}\frac{\left|\partial_n V|_0^{n+1}\right|^2}{4}\right)}_{=A_{0,0}} \psi_0^{n+1} + \underbrace{(-2)}_{=A_{0,1}}\psi_1^{n+1} + \underbrace{\frac{1}{2}}_{=A_{0,2}}\psi_2^{n+1} \\
&= \underbrace{\left(-g e^{i\mathcal{V}_0^{n+1}}\beta_1 e^{-i\mathcal{V}_0^{n}} - i\mathrm{sg}(\partial_n V|_0^{n+1})\frac{\sqrt{\left|\partial_n V|_0^{n+1}\right|}}{2} e^{i\mathcal{V}_0^{n+1}}\Delta t\Delta x \frac{\sqrt{|\partial_n V|_0^{n}|}}{2} e^{-i\mathcal{V}_0^{n}}\right)}_{=B_{0,0}} \psi_0^n \\
&+ \underbrace{\left[-g e^{i\mathcal{V}_0^{n+1}}\sum_{k=2}^{n+1}\left(\beta_k \psi_0^{n+1-k} e^{-i\mathcal{V}_0^{n+1-k}}\right) - i\mathrm{sg}(\partial_n V|_0^{n+1})\frac{\sqrt{\left|\partial_n V|_0^{n+1}\right|}}{2} e^{i\mathcal{V}_0^{n+1}}\Delta t\Delta x \sum_{k=1}^{n-1}\left(\frac{\sqrt{\left|\partial_n V|_0^{k}\right|}}{2} e^{-i\mathcal{V}_0^{k}}\psi_0^k\right)\right.}_{=S_0} \\
&\underbrace{\left. - i\mathrm{sg}(\partial_n V|_0^{n+1})\frac{\sqrt{\left|\partial_n V|_0^{n+1}\right|}}{2} e^{i\mathcal{V}_0^{n+1}}\frac{\Delta t\Delta x}{2}\frac{\sqrt{\left|\partial_n V|_0^{0}\right|}}{2} e^{-i\mathcal{V}_0^{0}}\psi_0^0\right]}_{=S_0}.
\end{aligned}$$

The formula is quite extensive; the reader will notice the right boundary scheme can be easily found using the following transformation of the **indices**, thanks to the symmetry of the 1D domain:

$$\begin{aligned} j: \quad & 0 \longmapsto J, \\ & 1 \longmapsto J-1, \\ & 2 \longmapsto J-2. \end{aligned}$$

A First Example of a Potential, No Boundary Interaction

Before showing the result obtained, we present an example with a strong attractive potential $\mathbb{V}(x,t) = V(x,t) = -2|x|^2$ placed at $x = 0$ so that the wave does not touch the boundary. This test is performed to check that the implementation of the potential is done correctly in the code.

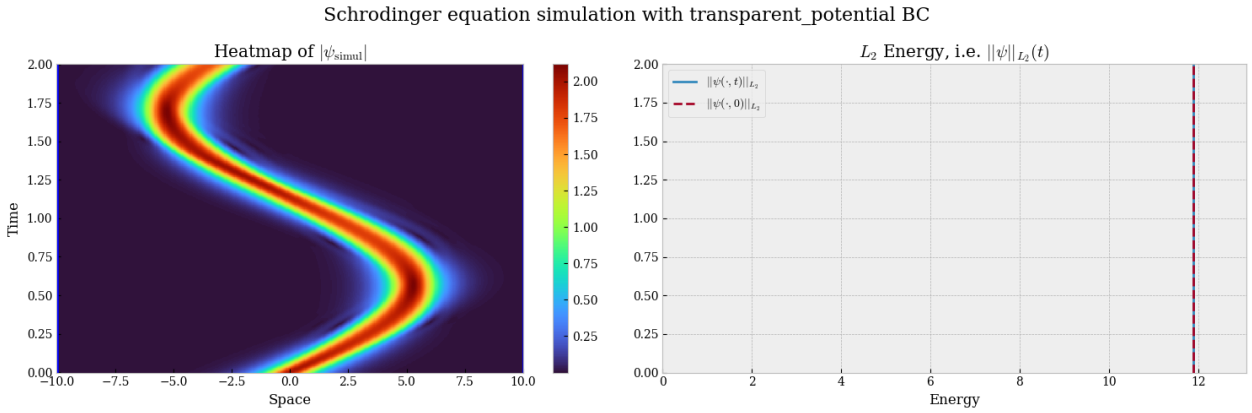

Figure 14: Simulation of (11) for Transparent Boundary Condition with $T = 2,501$ time points, $\Omega = [-10, 10]$, and 501 space points, strong potential.

It is possible to observe that the wave is indeed attracted by the potential, and its energy seems to remain stable, oscillating below its initial level. This behavior seems appropriate for the test case used here.

Repulsive Potential, Boundary Interaction

We now introduce a light repulsive potential with $\mathbb{V}(x,t) \equiv V(x,t) = 0.1|x|^2$ and let the wave impact the boundary. Below are two figures: the first one produced by a simulation using TBC for the homogeneous Schrödinger equation, which is inappropriate for this case, and the second one using the TBC designed in this subsection, which accounts for a non-zero potential.

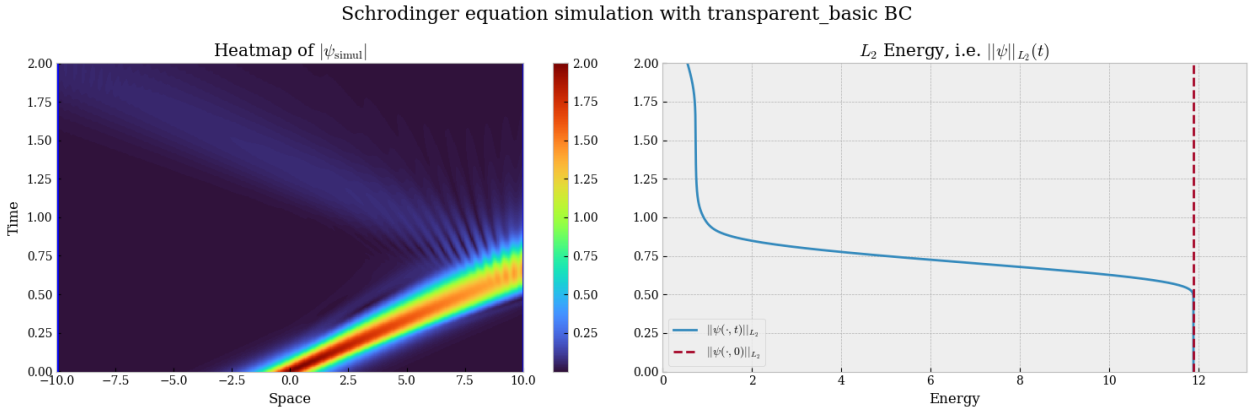

Figure 15: Simulation of (11) for Absorbing Boundary Condition for homogeneous Schrödinger equation, light repulsive potential.

There is no major difference as reflections can be observed in both cases. However, in the case of the TBC accounting for potential, the reflection is weaker than in the homogeneous TBC, which is quite positive.

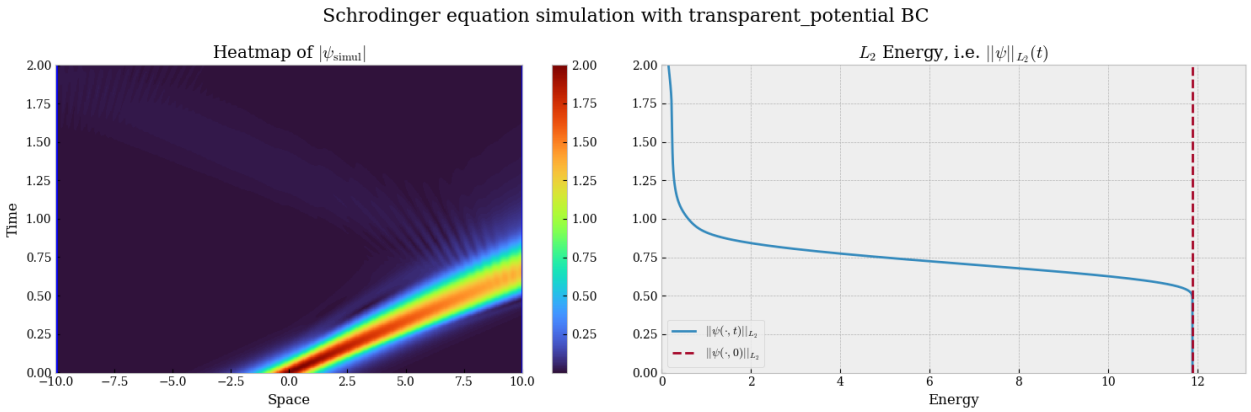

Figure 16: Simulation of (11) for Absorbing Boundary Condition accounting for potential, light repulsive potential.

3.5 Perfectly Matched Layers

The idea behind perfectly matched layers (PML) is to introduce an absorbing nonphysical layer $\Omega_{\text{PML}} := [-L^*, L^*] \setminus \Omega$ which surrounds the physical domain $\Omega = [-L, L]$, with $L^* = L + \delta$. To make this layer absorbing, we introduce a function Z which is constantly 1 in Ω and which dampens the waves in the outer layers Ω_{PML},

$$Z(x) = \begin{cases} 1 & \text{if } |x| \leq L, \\ 1 + e^{iv_x}\sigma_x(|x| - L^*) & \text{if } L < |x| \leq L^*, \end{cases} \tag{23}$$

where v_x is a constant and σ_x is the so-called absorbing function. By recommendation from [1], one sets $v_x = \frac{\pi}{4}$ and $\sigma_x = \sigma_0(x + \delta)^2$, where σ_0 is a constant controlling how aggressive the dampening is. This, together with the fact that $\delta = L^* - L$, gives us

$$Z(x) = \begin{cases} 1 & \text{if } |x| \leq L, \\ 1 + e^{\frac{i\pi}{4}}\sigma_0(|x| - L)^2 & \text{if } L < |x| \leq L^*. \end{cases} \tag{24}$$

Note that Z is continuous, specifically $\lim_{|x| \downarrow L} Z(x) = 1$.

To simplify the problem, we study PML for the Schrödinger equation with a zero potential ($\mathbb{V} \equiv 0$). Inserting this into eq. (11), our equation of interest is then

$$\begin{cases} \partial_t \psi^{\text{int}} - \frac{i}{2}\frac{\partial_x}{Z(x)}\left(\frac{\partial_x}{Z(x)}\right)\psi^{\text{int}} = 0 & (x,t) \in \Omega_T, \\ \psi^{\text{int}}(x,0) = \psi_0(x) & x \in \Omega. \end{cases} \tag{25}$$

To derive the corresponding Crank-Nicolson scheme, we simply divide by $Z(x)^2$ on the right-hand side and gain the scheme

$$\frac{\psi_j^{n+1} - \psi_j^n}{\Delta t} = \frac{c}{4(\Delta x)^2 Z(x)^2}\left[\left(\psi_{j+1}^{n+1} - 2\psi_j^{n+1} + \psi_{j-1}^{n+1}\right) + \left(\psi_{j+1}^n - 2\psi_j^n + \psi_{j1}^n\right)\right]. \tag{26}$$

In matrix form, this is expressed the same as in eqs. (13) and (14), but with a change in the constant C. Instead of $C = c\frac{\Delta t}{(\Delta x)^2}$, one sets $C = c\frac{\Delta t}{Z(x)^2(\Delta x)^2}$. Of course, this can be simplified, as $\frac{1}{Z(x)^2} \equiv 1$ for $x \in \Omega$, and thus for computational purposes the $\frac{1}{Z(x)^2}$ is only relevant to the cases where $|x| > L$. We start with simple Dirichlet boundary conditions, as the distinction between Dirichlet and Neumann conditions is not highly significant due to the dampening effect of Z. However, later, the results will be examined by applying ABC to the PML scheme.

The primary challenge in this context is to maintain a constant number of spatial discretization points, even as the simulation area expands. The objective is to operate with constant computational complexity. This means that the larger Ω_{PML} is, the less accurate the scheme in Ω will be, since more spatial discretization points are needed for the outer layer – which is not a part of our physical domain of interest.

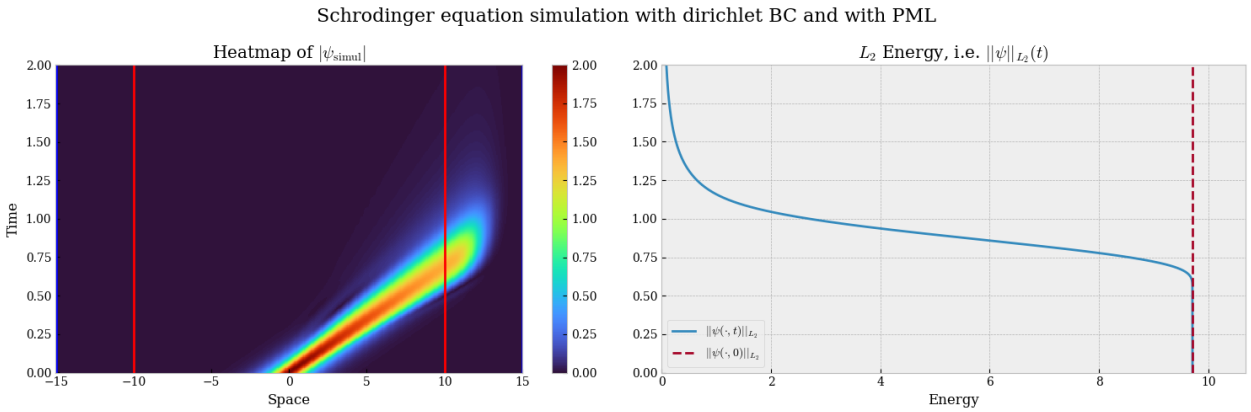

Figure 17: Simulation of (11) employing PML, with $[-15, 15]$ as the entire spatial simulation domain and $[-10, 10]$ as the region of interest.

Similar to the Absorbing Boundary Conditions (ABCs), the obtained results align with expectations, demonstrating a pronounced dissipation of energy at the boundary rather than within the domain, as seen in fig. 17. Further investigation into the method's accuracy is outlined in section 3.6. The results of the PML scheme is of course dependent on the choice of σ_0, where the optimal σ_0 depends on the function, the physical domain Ω and the size of the layer Ω_{PML}. A proper study of the optimal σ_0 is not done in this report, but if one wants to optimize the parameter, one could either aim to minimize the condition number for A or to minimize the error of the isolated reflections as seen in section 3.6.

3.6 Study of the Error

In this section, all simulation parameters are arbitrarily chosen. However, modifying them affects the results but not the presented trends. The focus is solely on the evolution of the system's results. For each TBC method discussed, an investigation is conducted analogous to the wave equation, examining the exact error and the isolated reflection to analyze boundary effects with the considered TBCs. The presentation of the material necessary to study the exact error is initiated. As demonstrated in appendix B.2.4, the exact solution to the homogeneous Schrödinger equation with the initial condition from the article [1], i.e.,

$$\forall x \in \mathbb{R}, \quad \psi_0(x) = 2\,\text{sech}(\sqrt{2}x)e^{i\frac{15}{2}x},$$

which can be expressed as

$$\forall t \geq 0, \forall x \in \mathbb{R}, \quad \psi(x,t) = e^{-i\frac{\pi}{4}} \frac{1}{\sqrt{4\pi t}} \left(2\,\text{sech}(\sqrt{2}z)e^{i\frac{15}{2}z} * \mathcal{G}_{-i/4t}(z)\right)(x),$$

where $\mathcal{G}_a := \exp(a||\cdot||^2)$ is the Gaussian kernel.

To implement this theoretical result, it is necessary to approximate the convolution. A Riemann formula is employed for this purpose to approximate the integral. The interval and the number of points for the approximation convolution computation are now also simulation parameters. However, once these values become large enough, they no longer have any influence. This is why further discussion on this matter will be omitted. The plot in fig. 18 illustrates the solution to our problem under the same parameters as before. Note that the exact solution resembles the results obtained during previous simulations. Regarding the exact error, the error measurement e_r is considered, as defined in (9).

Let's take a closer look at the reflection isolation method in the case of the wave equations. We are interested in focusing on reflections by separating them out for a detailed examination. Instead of only studying them by themselves, we want to compare their amplitude with respect to the original wave. This way, we can make sure they're not adding too much extra noise to our simulation. This careful look at reflections not only helps us understand them better but also makes sure our simulations are more accurate by keeping unwanted disruptions to a minimum. It enables to fine-tune the understanding of boundary effect for ABCs.

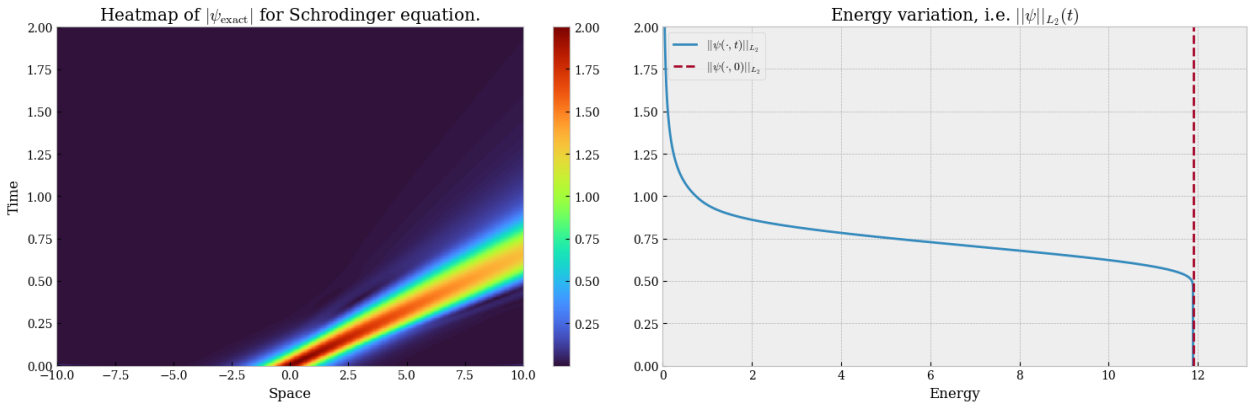

Figure 18: Exact solution of (11).

For this purpose, ψ is computed as before on Ω. The same simulation is then run on an extended version of the domain, with an additional segment of the size of Ω on each side to avoid reflection, giving ϕ. Reflections are then isolated, taking into account $\|\psi - \phi\|_\Omega$. For instance, if ψ is computed on $[-10, 10]$ with 501 space points, then ϕ would be computed on $[-30, 30]$ with $501 \times 3 - 2 = 1501$ space points. As a measure for this analysis, a new time $e_{r,i}$ is defined as (10).

3.6.1 ABC

In this section, we investigate the influence of ABCs alone, studying the error and undesired reflections as shown in fig. 13.

Exact Error

The exact error observed when applying ABCs is illustrated in fig. 19.

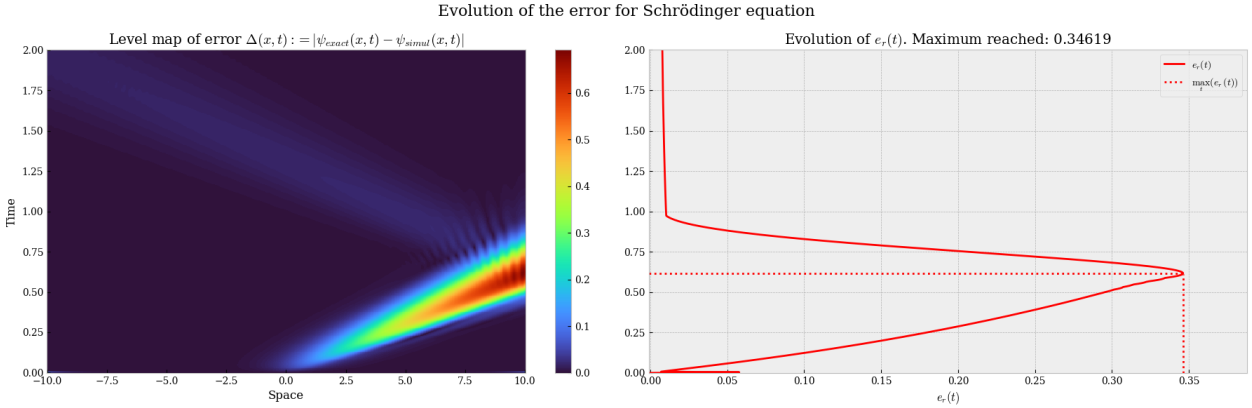

Figure 19: Exact error of (11) using ABCs.

An increasing error is observed in the simulation before reaching the boundary. This is attributed to a growing phase shift of the simulation concerning the exact solution. The manifestation of this is evident when examining the difference of norms, which is significantly smaller. While studying this phase shift is interesting, the primary objective is the investigation of boundary effects.

The method, in its current form, does not yield conclusive information about the effect of the edges, prompting the introduction of reflection isolation analysis initially. Nonetheless, it serves as a reference measure for the error committed by the discretization scheme of the equation with 501 discretization points in our physical zone of interest.

Isolating Reflections

Focusing on isolated reflections, as defined previously, we obtain the following figure, fig. 20.

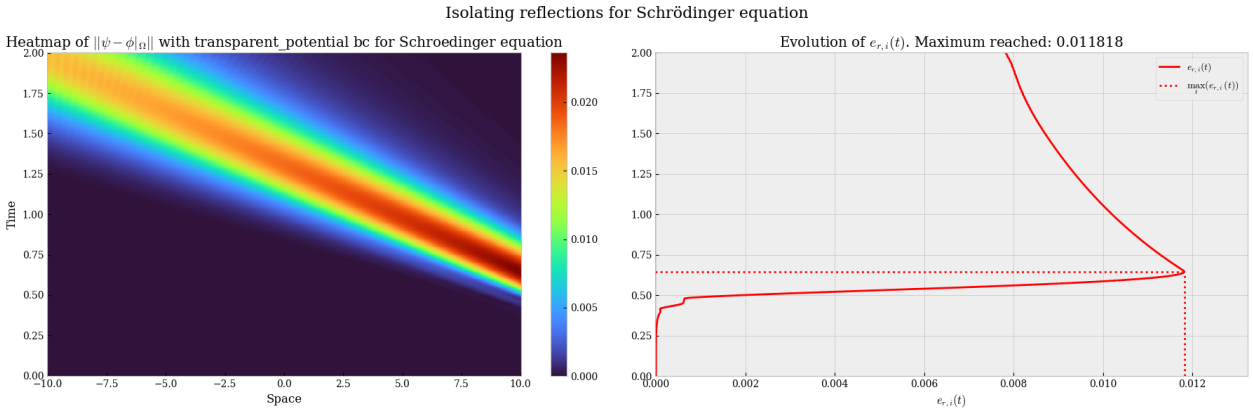

Figure 20: Isolated reflections of (11) using ABCs.

From this result, we can deduce that the error incurred by ABCs for the Schrödinger equation is similar to that for the wave equation. The amplitude of the reflections obtained with the use of the Transparent Boundary Condition is observed to be 100 times smaller than the original amplitude of the wave.

3.6.2 PML

We now examine the error made by the system applying PML, using Dirichlet boundary conditions and not ABCs. The objective is to evaluate the order of magnitude of the reflection on fig. 17.

Exact Error

The error made by the scheme is again of a higher order than the residues induced by the boundary conditions about reflections, here PMLs. This exact error, with the same parameters as when presenting the PMLs in fig. 17, is depicted in fig. 21.

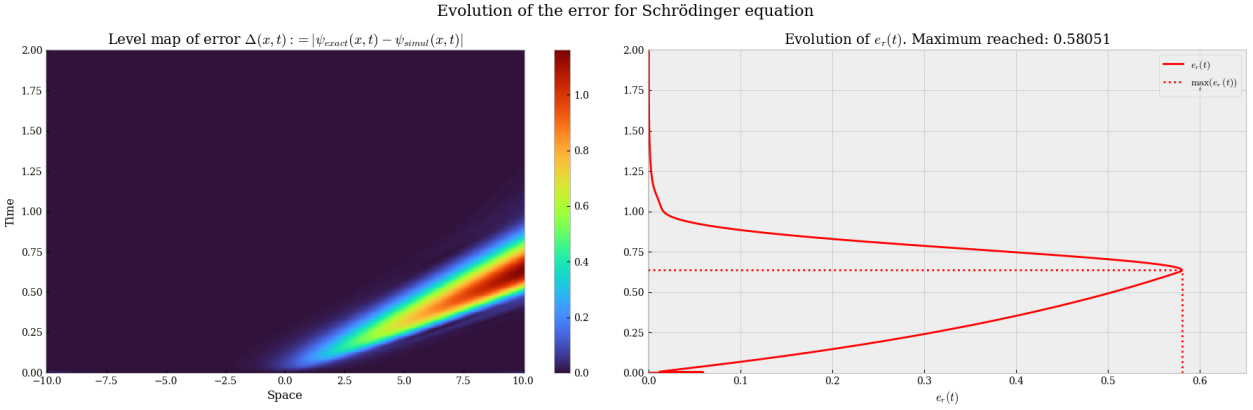

Figure 21: Exact error of (11) using PMLs with $[-15, 15]$ as the full space simulation domain and $[-10, 10]$ as the space of interest.

The cost of using PML manifests as a reduction in the number of space discretization points in the domain of interest, directly impacting the error. In fig. 21, considering an absorbing layer of width 5 on each side for a domain of interest of $[-10, 10]$, the size of the absorbing layers represents half of the total size. In this instance, this leaves 250 points for the domain of interest, which is half the discretization space of 501 points. This nearly multiplies the error e_r by two before reaching the edge of the domain of interest. However, the reflections seem to have a much less significant impact compared to ABCs. Thus, when using PML with fixed complexity, a trade-off arises between precision before and after reaching the inner edge. The parameter

associated with this dilemma is the width δ of the absorbing layers. With this adjustment, the damped layer is reduced to $[-10, 13]$, and the result is shown in fig. 22. With this, there is no additional hidden simulation on the left side and less on the right side. Note that this demands knowledge of the direction of propagation of the wave, which in this case is to the right.

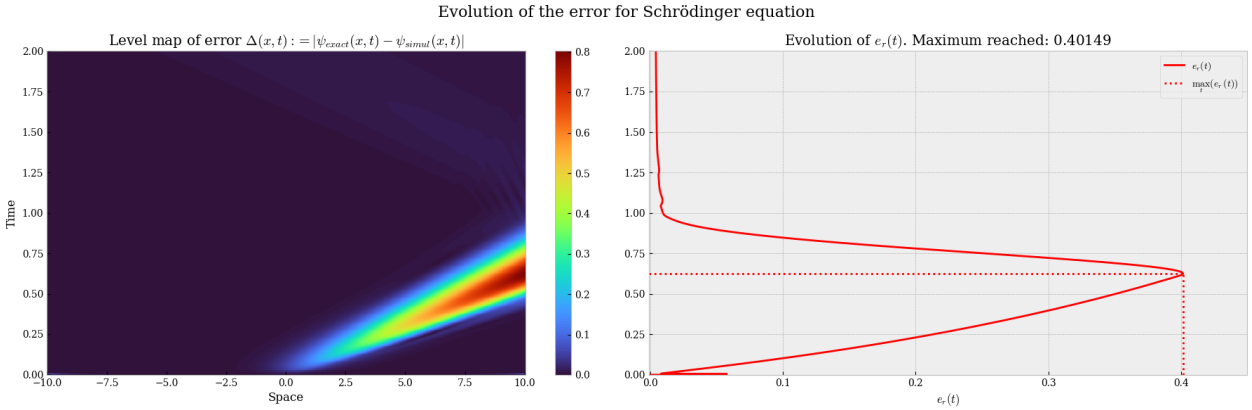

Figure 22: Exact error of (11) using PMLs with $[-10, 13]$ as the full space simulation domain and $[-10, 10]$ as the space of interest.

As expected, precision is regained in the primary simulation, with e_r at 0.40, which is much closer to what was found in the ABCs part. This adjustment also has an obvious impact on reflections. Nevertheless, the deliberate choice was made to keep the damped layer size small to emphasize the combination of ABCs and PMLs. However, the PML results alone are very satisfactory with a full domain size of $[-10, 14]$, yielding a maximum e_r at 0.42. Finally, as will be discussed in section 3.6.3, adding ABCs to PMLs improves the trade-off between the accuracy of the main equation simulation and that of the bounce.

Isolating Reflections

Isolating the reflections for the PML solution provides us with the results in fig. 23. From this, it can be

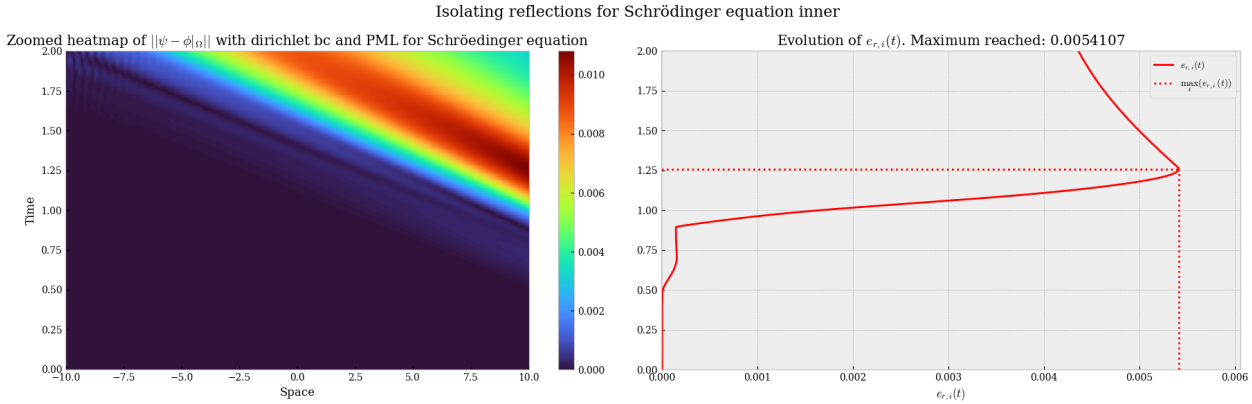

Figure 23: Isolated reflections of (11) using PMLs with $[-10, 13]$ as the full space simulation domain and $[-10, 10]$ as the space of interest.

inferred that the error incurred by PMLs in solving the Schrödinger equation is significantly lower compared to that for ABCs, decreasing from 1% to 0.5%. However, as explained previously, this excellent improvement in the reflections error is to the detriment of the precision of wave propagation. It could be interesting to evaluate the evolution of the error as a function of the thickness of the damping layers, though this study requires considerable computation time for typical computers.

3.6.3 ABC & PML

Paradigm

An idea to enhance the performance of the previously discussed trade-off is to reduce the width of absorbing layers and then add an ABC scheme to the outer edges of the simulation. This approach allows absorption of the wave on the outer edge but enables 99% of the latter to be absorbed. In other words, ABCs may be complementary to PMLs.

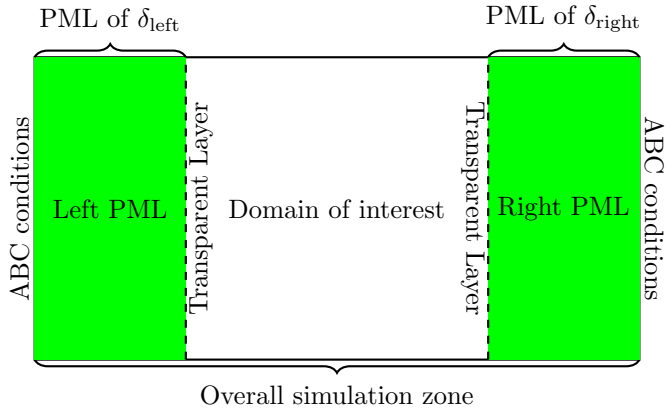

Figure 24: ABC & PML merged schemes.

The idea of the process is summarized in fig. 24. This aims to reduce the amount of energy across the PML zone so that the ABC conditions would lead to better absorption of the energy left. There is a trade-off between simulation complexity and precision of the simulation.

Exact Error

The exact error when considering the simultaneous use of ABCs and PMLs is illustrated in fig. 25.

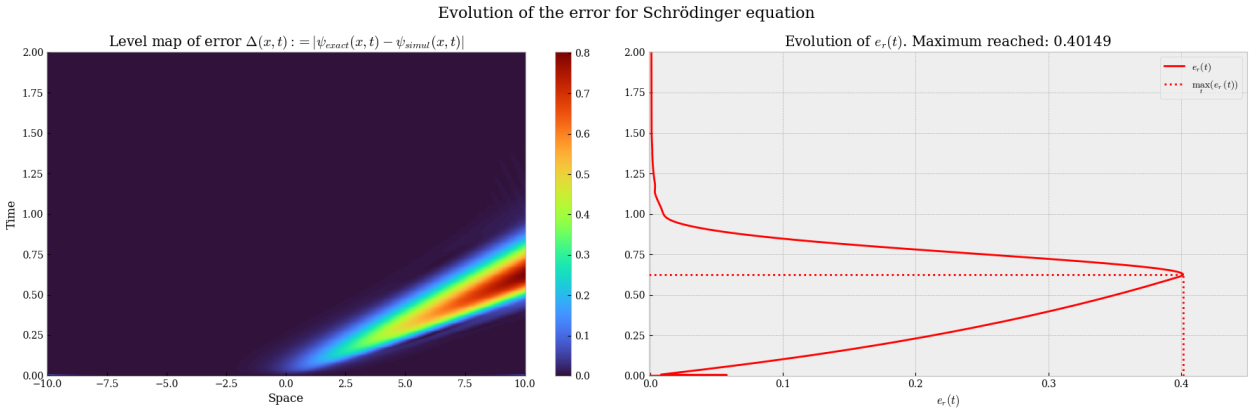

Figure 25: Exact error of (11) using ABCs and PMLs with $[-10, 13]$ as the full space simulation domain and $[-10, 10]$ as the space of interest.

As expected, a result extremely close to fig. 22 is obtained, with the difference that there seems to be less reflection. The error produced by the main scheme (before reaching the boundary) did not change, given that the number of discretization points in the space of interest did not change. Nelow we will conduct a study of the isolated reflections to obtain their orders of magnitude and measure the gain of ABCs added to PMLs.

Isolating Reflections

The result of isolating the reflections obtained by merging ABCs and PMLs is shown in fig. 26. It is very encouraging; adding ABCs to our previous PMLs scheme has an effect on reflection. The relative error goes from 1% for ABCs, to 0.5% for PMLs and finally 0.01% for ABCs and PMLs together, overall dividing the relative error by 100 by adding PMLs to ABCs and therefore by 10000 overall compared to the system without TBCs.

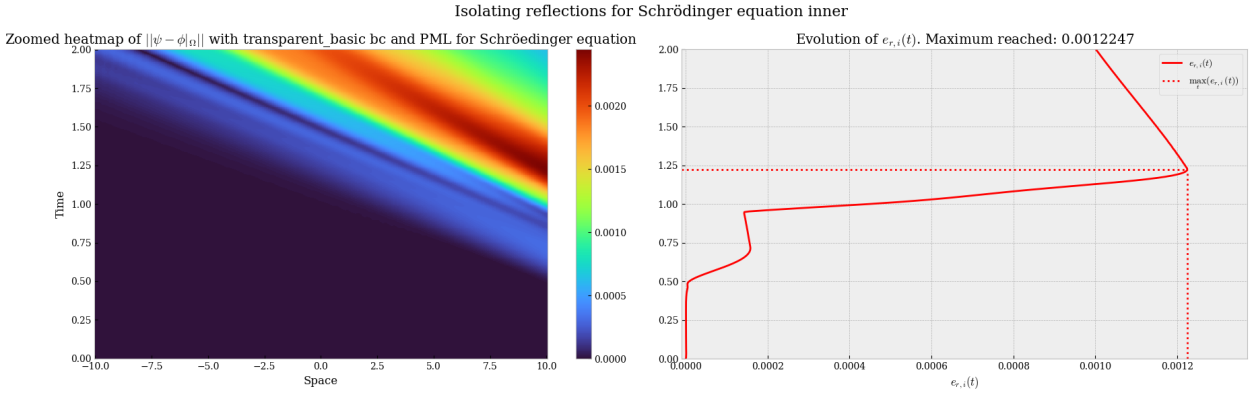

Figure 26: Isolated reflections of (11) using ABCs and PMLs with $[-10, 13]$ as the full space simulation domain and $[-10, 10]$ as the space of interest.

However, as explained, this has the effect of decreasing the accuracy of the main simulation of the equation. The key is to find a balance to meet the needs of the simulation. It would be interesting to conduct a more in-depth study on this dilemma. This study could prove to be very important when working, as has been done, with fixed complexity. In the case of very large simulations, it is essential to evaluate the addition of complexity induced by PMLs for a fixed accuracy.

Remark Note that in all the simulations presented here, the space and time steps are considered relatively high to highlight the effects of our TBCs, but the numerical results can be greatly improved by reducing them!

4 Conclusion

This study conducted a thorough exploration into solving the Schrödinger equation, with a specific focus on the influence of different boundary conditions, particularly Absorbing Boundary Conditions (ABCs) and Perfectly Matched Layers (PMLs). The primary goal was to understand the strengths and limitations of each method and investigate potential synergies arising from the combination of ABCs and PMLs.

4.1 Key Contributions

We delved into the exact error in the numerical implementation of the Schrödinger equation. The exact solution served as a benchmark, enabling a comprehensive evaluation of the performance of diverse boundary conditions. In addition, a method for isolating reflections, related to the exploration of wave equations, has been introduced. This facilitated the examination of the real amplitude and shape of reflections, offering valuable insights into their impact on the simulation.

A systematic analysis of the impact of ABCs and PMLs individually revealed that ABCs introduced a growing phase shift, and isolated reflections were significantly reduced in amplitude. PMLs exhibited lower errors compared to ABCs but introduced a trade-off between simulation accuracy before and after reaching the inner edge. To address this trade-off, a novel approach combining ABCs with PMLs was proposed. This hybrid approach has produced promising results, reducing reflections and improving overall accuracy, although it does lead to a moderate increase in computational complexity.

4.2 Achievements

The study demonstrated that the error introduced by PMLs was notably lower than that by ABCs. Moreover, the combination of ABCs and PMLs exhibited a substantial reduction in relative error, suggesting a potential solution to the accuracy-complexity trade-off.

4.3 Limitations

The study focused on specific parameters, and variations in simulation parameters could influence the observed results. Additionally, the trade-off between accuracy and computational complexity requires further exploration, especially in the context of larger simulations.

On one hand, the ABCs conditions can't be applied every time, especially when the potential has some non-linearity. For academic cases, this is fine, which is not necessarily the case for real-life applications. However, it produces very good results. On the other hand, the PML condition does not imply knowing the form of the wave. It introduces a damping layer to annihilate reflection without changing the scheme. Hence it can be done systematically. But it comes with a higher computational cost. That's why we saw the hybrid approach, which can be applied only if the Absorbing Boundary Conditions can be derived from the scheme.

4.4 Future Directions

Future work could involve a comprehensive study on the sensitivity of results to variations in simulation parameters. Investigating the impact of different widths of absorbing layers in PMLs on error and reflection reduction is another avenue for exploration. Furthermore, adaptive strategies for dynamically adjusting the width of absorbing layers based on evolving wave dynamics could be explored. Extending the analysis to more complex scenarios and larger simulations would also be valuable to assess scalability and generalizability.

With the same theory, one could write the equations in two dimensions. The process would be the same. One could expect similar results than the one presented in our work. This has been done in [1].

In conclusion, this study contributes valuable insights into the performance of boundary conditions for solving propagation equations, and especially the Schrödinger equation which was in the center of our study. The proposed combination of ABCs and PMLs presents opportunities for enhancing simulation accuracy in the presence of complex boundary effects. Identified limitations and future work directions pave the way for continued research in this domain.

5 Acknowledgements

We would like to express our sincere gratitude to our supervisors, Brigitte Bidegaray-Fesquet and Clément Jourdana, for their guidance and support throughout the project. Their attentiveness and dedication to helping us taught us a lot, and we greatly appreciate the opportunity to have benefited from their guidance.

Appendix

A Proof of Absorbing boundary conditions

A.1 ABCs for the wave equation

Let formulate the initial value problem associated to the wave equation,

$$\begin{cases} \partial_{tt}\psi - c^2\partial_{xx}\psi = 0 & \text{in} \quad \mathbb{R}\times(0,T), \\ \psi(\cdot,0) = \psi_0, \quad \partial_t\psi(\cdot,0) = \psi_{t,0} & \text{on} \quad \mathbb{R}. \end{cases} \tag{27}$$

It is proved in appendix B.1 that the solution of this problem takes the form of d'Alembert's formula (54),

$$\forall (x,t)\in\mathbb{R}\times(0,+\infty), \qquad \psi(x,t) = \frac{1}{2}[\psi_0(x+ct)+\psi_0(x-ct)] + \frac{1}{2c}\int_{x-ct}^{x+ct}\psi_{t,0}(y)\ \mathrm{d}y.$$

The aim now is to derive some 'far' space conditions from this analytical solution, so as to make the simulation more constrained with accurate boundary condition. We notice that we can therefore write

$$\psi(x,t) = \psi^l(x+ct) + \psi^r(x-ct)$$

with

$$\psi^l(x) = \frac{1}{2}\left(\psi_0(x) + \int_{-\infty}^{x}\psi_{t,0}(u)\ \mathrm{d}u\right) \qquad \text{and} \qquad \psi^r(x) = \frac{1}{2}\left(\psi_0(x) - \int_{x}^{+\infty}\psi_{t,0}(u)\ \mathrm{d}u\right).$$

In the following, we will assume that ψ_0 and $\psi_{t,0}$ are compactly supported and bounded, note that if $\psi_{t,0}$ is in $L_1(\mathbb{R})$, so the quantities ψ^l and ψ^r are well defined on $\mathbb{R}$. Let's study the temporal behavior of the solution 'far' in space. For example, let's move to the left of the x-axis, we introduce $\mathbb{R}_l = \{x\in\mathbb{R}\ /\ x < \inf\left(\bigcup \mathrm{supp}(\psi_0,\psi_{t,0})\right)\}$ and observe that

$$\forall x\in\mathbb{R}_l, \qquad \psi^r(x) = 0.$$

The main property of this set is that for $x\in\mathbb{R}^l$ and all $t>0$, we have $x-ct\in\mathbb{R}_l$ and then $\psi^r(x-ct)=0$. The time evolution of a point x on the left can be summarized as follows,

$$\forall (x,t)\in\mathbb{R}_l\times(0,T), \qquad \psi(x,t) = \psi^l(x+ct). \tag{28}$$

Noting that $\partial_x\psi|_{x\in\mathbb{R}^l}(x,t) = [\psi^l]'(x+ct)$, it comes

$$\begin{aligned} \forall (x,t)\in\mathbb{R}_l\times(0,T), \qquad \partial_t\psi(x,t) &\overset{(28)}{=} \partial_t\psi^l(x+ct) \\ &\overset{\text{chain rule}}{=} c[\psi^l]'(x+ct) \\ &= c\partial_x\psi(x,t). \end{aligned} \tag{29}$$

On the same principle, we can do exactly the same thing on the right $\mathbb{R}_r = \{x\in\mathbb{R}\ /\ x > \sup\left(\bigcup\mathrm{supp}((\psi_0,\psi_{t,0}))\right)\}$ and deduce that

$$\forall (x,t)\in\mathbb{R}_r\times(0,T), \qquad \partial_t\psi(x,t) = -c\partial_x\psi(x,t). \tag{30}$$

Equations (29) and (30) can be unified for x 'far' (more formally defined as $\mathbb{R}_r\cup\mathbb{R}_l$) as

$$\partial_n\psi + \frac{1}{c}\partial_t\psi = 0, \tag{31}$$

where n is the outwardly unit normal vector (i.e $+1$ for right and -1 for left) and then ∂_n the normal derivative. Since this equation a direct consequence of (27), we can add it to our equations system without loss of generality:

$$(27) \iff \begin{cases} \partial_{tt}\psi - c^2\partial_{xx}\psi = 0 & \text{in} \quad \mathbb{R}\times(0,T), \\ \psi(\cdot,0) = \psi_0, \quad \partial_t\psi(\cdot,0) = \psi_{t,0} & \text{on} \quad \mathbb{R}, \\ \partial_n\psi(x,t) + \frac{1}{c}\partial_t\psi(x,t) = 0 & \text{on} \quad \mathbb{R}^r\cup\mathbb{R}^l\times(0,T). \end{cases}$$

Let's get back to the problem of boundary space conditions during simulation. Let us therefore restrict the problem on $\Omega\times[0,T]$, where Ω is a closed set of $\mathbb{R}$, our problem becomes

$$\begin{cases} \partial_{tt}\psi - c^2\partial_{xx}\psi = 0 & \text{in} \quad \Omega\times(0,T), \\ \psi(\cdot,0) = \psi_0, \quad \partial_t\psi(\cdot,0) = \psi_{t,0} & \text{on} \quad \Omega, \\ \partial_n\psi(x,t) + \frac{1}{c}\partial_t\psi(x,t) = 0 & \text{on} \quad \partial\Omega\times[0,T], \end{cases}$$

Note that the added equation intuitively allows us to dictate the boundary behaviour of the simulation so that the function is not reflected or whatever. This is why equation (31) is named Absorbing Boundary Condition (ABC) equation.

A.2 ABCs for Schrödinger equation

We are going to prove the ABCs derived pages 6 and 7 in [1], introducing all needed hypothesis on the concerned functions.

A.2.1 Notations and problem

The computational space domain is denoted $\Omega \subset \mathbb{R}$ which is closed and bounded, which boundary is denoted Σ. In the case of the 1D Schrödinger equation, the left and right complementary spaces are respectively denoted $\Omega_l := [-\infty, x_l]$ and $\Omega_r := [x_r, +\infty[$, with $\Omega_{l,r} := \Omega_l \cup \Omega_r$ such that $\Omega \cup \Omega_{\ell,r} = \mathbb{C}$. With these notations, $\Sigma = \{x_l, x_r\}$ and we set $\Sigma_T = \partial\Omega \times [0, T]$, T being the period of time on which we look for solutions. The authors introduce the problem as a couple transmission problem as follows :

$$\begin{cases} \left(i\partial_t + \partial_x^2\right)\psi^{\text{int}} = 0, x \in \Omega, t > 0 & \text{(32a)} \\ \partial_x\psi^{\text{int}} = \partial_x\psi^{\text{ext}}, x \in \Sigma, t > 0 & \text{(32b)} \\ \psi^{\text{int}}(x, 0) = \psi_0(x), x \in \Omega & \text{(32c)} \end{cases}$$

and

$$\begin{cases} \left(i\partial_t + \partial_x^2\right)\psi^{\text{ext}} = 0, x \in \Omega_{\ell,r}, t > 0 & \text{(33a)} \\ \psi^{\text{ext}} = \psi^{\text{int}}, x \in \Sigma, t > 0 & \text{(33b)} \\ \lim\limits_{|x|\to\infty} \psi^{\text{ext}}(x, t) = 0, t > 0 & \text{(33c)} \\ \psi^{\text{ext}}(x, 0) = 0, x \in \Omega_{\ell,r}. & \text{(33d)} \end{cases}$$

This formulation makes sense as one could see the problem as finding a compactly supported function on Ω (32c), (33c), obeying Schrödinger equation on $\mathbb{R}$ (33a), (32a), $\mathcal{C}^1$ on spatial domain (32b), (33b), with initial condition (33d) that could for instance have the shape

$$\psi(x, t) = \psi^{\text{int}}(x, t)\mathbb{1}_\Omega(x, t) + \psi^{\text{ext}}(x, t)\mathbb{1}_{\Omega_{\ell,r}}(x, t)$$

with some initial condition (32c), (33d). That way, the boundary of computational domain is involved in the computation, enabling to find new conditions on it.

A.2.2 Laplace transform on coupled transmission problem

Start by applying Laplace transform (LT) on equation (33a). Recall the Laplace transform of a function $f(t) \in L^2(\mathbb{R}^+, \mathbb{C})$ is defined for $\omega \in \mathbb{C}$ as:

$$\hat{f}(w) := \mathcal{L}[f](w) = \int_{t=0}^{\infty} f(t)e^{-\omega t}\, \mathrm{d}t$$

It can be shown that this is a reversible operation on $L^2(\mathbb{R}^+, \mathbb{C})$, and the integral converges absolutely for $\Re(\omega) > \inf\{\sigma = \Re(z), z \in \mathbb{C} \mid \mathcal{L}[f](\sigma) \text{ converges absolutely}\}$. In our case, we assume $\psi^{\text{ext}}(x, .) \in L^2(\mathbb{R}^+, \mathbb{C})$ since Laplace transform is reversible for such kind of functions. The Laplace transform of the function is thus well defined, and we get absolute convergence of the LT as soon as $\Re(w) > 0$ since $\psi^{\text{ext}}(x, .) \in L^2(\mathbb{R}^+, \mathbb{C})$ (using Cauchy-Schwarz inequality).

$$\begin{aligned} \int_{t=0}^{\infty} \left(i\partial_t\psi^{\text{ext}} + \partial_x^2\psi^{\text{ext}}\right)e^{-t\omega}\, \mathrm{d}t &= i\int_{t=0}^{\infty} \partial_t\psi^{\text{ext}}e^{-t\omega}dt + \partial_x^2\int_{t=0}^{\infty} \psi^{ext}e^{-\omega t}\, \mathrm{d}t \\ &\overset{IBP}{=} i\left(\left[\psi^{ext}e^{-t\omega}\right]_0^{\infty} + \int_{t=0}^{\infty} \omega\psi^{ext}e^{-t\omega}\, \mathrm{d}t\right) + \partial_x^2\hat{\psi}^{\text{ext}}(x, \omega) \\ &= i\omega\hat{\psi}^{\text{ext}}(x, \omega) + \partial_x^2\hat{\psi}^{\text{ext}}(x, \omega) \\ &= 0. \end{aligned}$$

Note that $[\psi^{ext}e^{-t\omega}]_0^{\infty} = 0$ because of (33d) and absolute convergence. We now are in possession of a brand new ODE :

$$i\omega\hat{\psi}^{\text{ext}}(x, \omega) + \partial_x^2\hat{\psi}^{\text{ext}}(x, \omega) = 0 \tag{34}$$

which admits a unique solution, for example, on Ω_r, given by :

$$\hat{\psi}^{ext}(x,\omega) = A^+(\omega)e^{\sqrt[+]{-i\omega}x} + A^-(\omega)e^{-\sqrt[+]{-i\omega}x} \tag{35}$$

where $\Re(\sqrt[+]{\cdot}) > 0$ so that absolute convergence of the integral can be maintained, thus its well-definiteness. For instance, apply Laplace transform on (33c) :

$$\begin{aligned}
&\lim_{|x|\to\infty} \psi^{\text{ext}}(x,t) = 0 \\
\iff &\int_{t=0}^{\infty} \lim_{|x|\to\infty} \psi^{\text{ext}}(x,t)e^{-\omega t}\,\mathrm{d}t = 0 \\
\implies &\lim_{|x|\to\infty} \int_{t=0}^{\infty} \psi^{\text{ext}}(x,t)e^{-\omega t}\,\mathrm{d}t = 0, \text{ dominated convergence} \\
\iff &\lim_{x_r\to+\infty} \hat{\psi}^{\text{ext}}(x,\omega) = 0, \text{ by definition of Laplace transform, and } -\infty < x_r \\
\implies &A^+(\omega) = 0.
\end{aligned}$$

From now on, we keep, for $(x,\omega) \in \Omega_r \times \mathbb{C}$, $\hat{\psi}^{\text{ext}}(x,w) = A^-(\omega)e^{-\sqrt[+]{-iw}x}$.

A.2.3 Link solution to external problem with internal problem

We start by re-expressing the previously found solution to get rid of the coefficient $A^-(\omega)$:

$$\hat{\psi}^{\text{ext}}(x,w) = e^{-\sqrt[+]{-iw}(x-x_r)}e^{-\sqrt[+]{-iw}x_r}A^-(\omega) = e^{-\sqrt[+]{-iw}(x-x_r)}\hat{\psi}^{\text{ext}}(x_r,w) \tag{36}$$

The expression can then be differentiated with respect to x so that

$$\begin{aligned}
\partial_x\hat{\psi}^{\text{ext}}(x,\omega) &= -\sqrt[+]{-iw}\hat{\psi}^{\text{ext}}(x_r,\omega)e^{-\sqrt[+]{-iw}(x-x_r)} &(37)\\
&= -\sqrt[+]{-iw}\hat{\psi}^{\text{int}}(x_r,\omega)e^{-\sqrt[+]{-iw}(x-x_r)}, \text{ using (33b)} &(38)\\
&= \partial_x\hat{\psi}^{\text{int}}(x,\omega) &(39)
\end{aligned}$$

where $x \in \Sigma \cap \Omega_r$ because of the last step we performed. Then $\partial_x\hat{\psi}^{\text{int}}(x,\omega)\Big|_{x=x_r} = -\sqrt[+]{-i}w\frac{\hat{\psi}^{\text{int}}(x_r,\omega)\big|_{x=x_r}}{\sqrt{w}}$. We need to compute $-\sqrt[+]{-i}$. Using $i = e^{i\frac{\pi}{2}}$ leads to $\Re(\sqrt{-i}) = -\frac{\sqrt{2}}{2} < 0$, thus we use $-i = e^{-i\frac{\pi}{2}}$ leading to $\Re(\sqrt{-i}) = \frac{\sqrt{2}}{2} > 0$ so that $\sqrt[+]{-i} = e^{-i\frac{\pi}{4}}$. At this point, we have :

$$\partial_x\hat{\psi}^{\text{int}}(x,\omega)\Big|_{x=x_r} = -e^{-i\frac{\pi}{4}}w\frac{\hat{\psi}^{\text{int}}(x_r,\omega)\Big|_{x=x_r}}{\sqrt{w}} \tag{40}$$

A.2.4 Get back to original transmission problem with inverse Laplace transform

As we are working on spaces where Laplace transform can be inverted, we apply it to the very last relation we got on $\partial_x\hat{\psi}^{\text{int}}$. As no explicit formula for such operation exists, we will use LT properties :

Prop.	$f(t)$	$\mathcal{L}[f](\omega) = F(\omega)$
1	$f'(t)$	$\omega F(\omega) - f(0)$
2	$(f*g)(t)$	$F(\omega)G(\omega)$
3	$t \mapsto t^\alpha, \Re(\alpha) > -1$	$\frac{\Gamma(\alpha+1)}{\omega^{\alpha+1}}$

We can write $\partial_x\hat{\psi}^{\text{int}}(x,\omega)\Big|_{x=x_r}$ as the product of two functions such as :

$$\partial_x\hat{\psi}^{\text{int}}(x,\omega)\Big|_{x=x_r} = \frac{-e^{-i\frac{\pi}{4}}}{\sqrt{w}} \cdot w\ \hat{\psi}^{\text{int}}(x_r,\omega)\Big|_{x=x_r} \tag{41}$$

$$\overset{\text{prop. 2}}{\implies} \partial_x\psi^{\text{int}}(x,t)\big|_{x=x_r} = \mathcal{L}^{-1}\left[\frac{-e^{-i\frac{\pi}{4}}}{\sqrt{w}}\right] * \mathcal{L}^{-1}\left[w\ \hat{\psi}^{\text{int}}(x_r,\omega)\Big|_{x=x_r}\right](t) \tag{42}$$

Property 3 can be reformulated as $\mathcal{L}\left[t \mapsto \frac{t^\alpha}{\Gamma(\alpha+1)}\right](\omega) = \frac{1}{w^{\alpha+1}}$ thus $\mathcal{L}^{-1}\left[\frac{-e^{-i\frac{\pi}{4}}}{\sqrt{w}}\right](t) = \frac{-e^{-i\frac{\pi}{4}}}{\sqrt{\pi}}\frac{1}{\sqrt{t}}$. Using the fact that $\psi^{\text{int}}\big|_{\Sigma_T} = 0$, presented page 2 of [1], we get that $\psi^{\text{int}}(x_r, 0) = 0$ thus applying prop. 3 leads to $\mathcal{L}^{-1}\left[w\ \hat{\psi}^{\text{int}}(x_r,\omega)\Big|_{x=x_r}\right](t) = \partial_t\psi^{\text{int}}(x,t)\big|_{x=x_r}$. This means that equation (42) yields

$$\partial_x\psi^{\text{int}}(x,t)\big|_{x=x_r} = \frac{-e^{-i\frac{\pi}{4}}}{\sqrt{\pi}}\frac{1}{\sqrt{t}} * \partial_t\psi^{\text{int}}(x,t)\big|_{x=x_r}(t) \tag{43}$$

$$= -e^{-i\frac{\pi}{4}}\partial_t\left(\frac{1}{\sqrt{\pi}}\int_{s=0}^{t}\frac{\psi^{\text{int}}(x,s)\big|_{x=x_r}}{\sqrt{t-s}}\,\mathrm{d}s\right) \tag{44}$$

$$= -e^{-i\frac{\pi}{4}}\partial_t^{1/2}\psi^{\text{int}}(x_r,s) \text{ (Caputo fractional derivative definition)} \tag{45}$$

Thanks to the symmetry of the notation, the same expression can be derived on the external domain Ω_ℓ, which can be concatenated into the formulation

$$\left(\partial_n + e^{-i\frac{\pi}{4}}\partial_t^{1/2}\right)\psi^{\text{int}} = 0, \text{ on } \Sigma_T = \{x_\ell, x_r\}\times[0,T] \tag{46}$$

B Theoretical point and resolution of PDEs

The purpose of this section is to focus on the analytical resolution of certain PDEs, with the aim of evaluating our simulations and presenting some interesting PDE resolution methods. We recommend the Lawrence C. Evans' book [3], it offers a clear and thorough exposition of the fundamental concepts and resolutions of partial differential equations.

B.1 Wave equation

We are going to rule on the d'Alembert's formula which is the solution of the homogeneous one-dimensional wave equation with constant speed. Let's start by recalling the PDE (27),

$$\begin{cases} \partial_{tt}\psi - c^2\partial_{xx}\psi = 0 & \text{in} \quad \mathbb{R}\times(0,+\infty), \\ \psi(\cdot,0) = \psi_0, \quad \partial_t\psi(\cdot,0) = \psi_{t,0} & \text{on} \quad \mathbb{R}. \end{cases} \tag{47}$$

Let's begin by observing that the partial differential equation can be expressed in a "factored" form as follows,

$$(\partial_t + c\partial_x)(\partial_t - c\partial_x)\psi = 0 \tag{48}$$

For all x real and t positive, defining the relation $\phi(x,t) := (\partial_t - c\partial_x)\psi(x,t)$, equation (48) can be rewritten

$$\partial_t\phi + c\partial_x\phi = 0 \tag{49}$$

This is a transport equation with a constant coefficient. Let's digress for a moment to solve this equation.

B.1.1 Homogeneous transport equation with constant coefficients

We search a function ϕ such that

$$\begin{cases} \partial_t\phi + c\partial_x\phi = 0, & (x,t)\in\mathbb{R}\times(0,+\infty), \\ \phi(x,0) = \phi_0(x), & x\in\mathbb{R}. \end{cases} \tag{50}$$

We'll take the opportunity of solving this equation to present the method of characteristics. The main idea is to define the characteristic lines along which the partial differential equation reduces to a simple ordinary differential equation. Solving the ordinary differential equation along a characteristic line enables us to find the solution to the original problem.

Let's define, for fixed $(x,t)\in\mathbb{R}\times(0,\infty)$, such a parametric characteristic curve $(x(s),t(s))$ for $s\in(0,T)$ such that $x(0)=x$ and $t(0)=t$, in other word we follow a particle which is at position x at time t. It follows from these choices

$$\partial_s\phi(x(s),t(s)) = \partial_x\phi(x(s),t(s))x'(s) + \partial_t\phi(x(s),t(s))t'(s).$$

We choose $x'(s)=c$ and $t'(s)=1$ to recover our initial equation,

$$\begin{aligned} \forall s\in(0,+\infty), \quad \partial_s\phi(s) = c\partial_x\phi(s) + \partial_t\phi(s) &\overset{(50)}{=} 0 \\ \Rightarrow \quad \phi(s) &= \phi(x(0),t(0)). \end{aligned}$$

That also implies for $s\geq 0$, $x(s)=cs+x$ and $t(s)=t+s$, which involves $x=x-ct$. We finally get, for all $s\in\mathbb{R}$, that $\phi(s)$ is a constant. By applying at $s=-t$ it comes

$$\forall s\in\mathbb{R}, \quad \phi(s) = \phi(x(-t),t(-t)) = \phi(x-ct,0) = \phi_0(x-ct).$$

In conclusion,

$$\forall(x,t)\in\mathbb{R}\times(0,+\infty), \qquad \phi(x,t) = \phi_0(x-ct).$$

□

Let's go back to our one-dimensional wave equation, we have therefore the solution of equation (49)

$$\forall(x,t)\in\mathbb{R}\times(0,+\infty), \qquad \phi(x,t) := (\partial_t - c\partial_x)\psi(x,t) = \phi_0(x-ct). \tag{51}$$

Moreover,

$$\forall x\in\mathbb{R}, \qquad \phi_0(x) = \phi(x,0) = \partial_t\psi(x,0) - c\partial_x\psi(x,0). \tag{52}$$

The equation (51) is a nonhomogoneous transport equation, let's present a resolution of this kind of equation.

B.1.2 Nonhomogeneous transport equation with constant coefficients

Now, we search a function ψ such that

$$\begin{cases} \partial_t \psi - c\partial_x \psi = \xi, & (x,t) \in \mathbb{R} \times (0,+\infty), \\ \psi = \psi_0, & (x,t) \in \mathbb{R} \times \{0\}. \end{cases} \tag{53}$$

Inspired by the previous method, we fix $(x,t) \in \mathbb{R} \times (0,+\infty)$ and define our parametric curve $x(s), t(s) := (x - cs, t + s)$ for $s \in \mathbb{R}$. To facilitate our notation, let's introduce the function ζ by $\zeta(s) := \psi(x - cs, t + s)$ for $s \in \mathbb{R}$. We note that $\zeta(0) = \psi(x,t)$ and $\zeta(-t) = \psi(x + ct, 0)$. It comes,

$$\forall s \in \mathbb{R}, \qquad \zeta'(s) = -c\partial_x \psi(x - cs, t + s) + \partial_t \psi(x - cs, t + s) = \xi(x - cs, t + s).$$

We remark that

$$\begin{aligned} \int_{-t}^{0} \zeta'(s)\ \mathrm{d}s = \zeta(0) - \zeta(-t) &= \psi(x,t) - \psi(x + ct, 0) \\ \Rightarrow \qquad \psi(x,t) &= \int_{-t}^{0} \xi(x - cs, t + s)\ \mathrm{d}s + \psi_0(x + ct) \\ \Rightarrow \qquad \psi(x,t) &= \int_{0}^{t} \xi(x - c(s - t), s)\ \mathrm{d}s + \psi_0(x + ct). \end{aligned}$$

We conclude this paragraph by stating that $(x,t) \in \mathbb{R} \times (0,+\infty) + \mapsto \int_0^t \xi(x - c(s - t), s)\ \mathrm{d}s + \psi_0(x + ct)$ is the solution to problem (53).

□

We now have all the tools we need to solve the one-dimensional wave equation (47).
It comes by solving (51)

$$\begin{aligned} \forall (x,t) \in \mathbb{R} \times (0,+\infty), \qquad \psi(x,t) &= \int_0^t \phi_0(x - c(s - t) - cs)\ \mathrm{d}s + \psi_0(x + ct) \\ &= \int_0^t \phi_0(x + ct - 2cs)\ \mathrm{d}s + \psi_0(x + ct) \\ &= \frac{1}{2c} \int_{x-ct}^{x+ct} \phi_0(y)\ \mathrm{d}y + \psi_0(x + ct) \end{aligned}$$

By injecting the equation (52) it comes

$$\begin{aligned} \forall (x,t) \in \mathbb{R} \times (0,+\infty), \qquad \psi(x,t) &= \frac{1}{2c} \int_{x-ct}^{x+ct} \left[\partial_t \psi(y,0) - c\partial_x \psi(y,0)\right]\ \mathrm{d}y + \psi_0(x + ct) \\ &= \frac{1}{2c} \int_{x-ct}^{x+ct} \partial_t \psi(y,0)\ \mathrm{d}y - \frac{1}{2}\left[\psi_0(x + ct) - \psi_0(x - ct, 0)\right] + \psi_0(x + ct) \end{aligned}$$

So we have d'Alembert's formula which is solution of (47),

$$\forall (x,t) \in \mathbb{R} \times (0,+\infty), \qquad \psi(x,t) = \frac{1}{2}[\psi_0(x + ct) + \psi_0(x - ct)] + \frac{1}{2c} \int_{x-ct}^{x+ct} \psi_{t,0}(y)\ \mathrm{d}y. \tag{54}$$

B.2 Homogeneous Schrödinger equation

Here we are interested in solving homogeneous Schrödinger equation on $\mathbb{R}$.

$$\begin{cases} \partial_t \psi - i\partial_{xx} \psi = 0 & \text{in} \quad \mathbb{R} \times (0,+\infty), \\ \psi(\cdot, 0) = \psi_0 & \text{on} \quad \mathbb{R}. \end{cases} \tag{55}$$

In order to solve it, always with the aim of presenting a wide range of methods, we will use Fourier theory. The method presented here is inspired of the resolution of diffusion equation by using Fourier transform. There are numerous other methods to solve this equation; for example, we can mention the method of deriving the fundamental form as presented in *2.3.1* of [3].

Before presenting our demonstration, we find it interesting to provide a theoretical overview of the Fourier transform and related concepts to establish a consistent framework for our study.

B.2.1 A brief introduction to the Fourier transform framework

In his book *Theory of Distributions and Fourier Analysis* [4], Jean-Michel Bony provides a detailed exploration of the intricacies of the Fourier transformation. Proofs of the results used in this section can be found in this book. Naturally, let's start by introducing the Fourier transform.

Definition B.2.1. Fourier Transform
*Let $f \in L^1(\mathbb{R})$, the **Fourier transform** (FT) of f is defined as the function $\tilde{f}$ on $\mathbb{R}$ by:*

$$\mathcal{F}(f)(\xi) = \tilde{f}(\xi) := \int_{\mathbb{R}} f(x) e^{-2i\pi x\cdot\xi} \, \mathrm{d}x$$

We will now intuitively introduce the notion of Schwartz space, a fundamental set of Fourier theory. Remaining in an L^1 frame, if f is sufficiently derivable with its derivatives in L^1 then we obtain for $\alpha \in \mathbb{N}$,

$$\mathcal{F}(\partial_x^\alpha f)(\xi) = \int_{\mathbb{R}} \partial_x^\alpha f(x) e^{-2i\pi x\cdot\xi} \, \mathrm{d}x \overset{IBP}{=} (2i\pi\xi)^\alpha \mathcal{F}(f)(\xi) \tag{56}$$

If, analogously, $x^\alpha f \in L^1$ and $\tilde{f}$ is sufficiently differentiable, by derivation through the fundamental theorem of calculus

$$\partial_\xi^\alpha \tilde{f}(\xi) = \partial_\xi^\alpha \left(\int_{\mathbb{R}^d} f(x) e^{-2i\pi x\cdot\xi} \, \mathrm{d}x \right) = \mathcal{F}\left((-2i\pi x)^\alpha f \right)(\xi) \tag{57}$$

We come to understand the fundamental observation that the Fourier transformation interchanges regularity (in terms of differentiability) and decay (in a polynomial sense) at infinity. This observation serves as motivation for defining the Schwartz space.

Definition B.2.2. Schwartz space and rapid decay
Let $f : \mathbb{R} \longrightarrow \mathbb{R}$. f is said to have "rapid decay" if:

$$\forall p \in \mathbb{N}, \quad \lim_{|x|\to+\infty} x^p f(x) = 0$$

The Schwartz space, denoted $\mathcal{S}(\mathbb{R})$, is defined as the set of functions $f : \mathbb{R} \longrightarrow \mathbb{R}$ such that:

1. *$f \in \mathcal{C}^\infty(\mathbb{R})$;*
2. *$\forall p \in \mathbb{N}$, $f^{(p)}$ has rapid decay.*

We have the following fundamental result.

Lemma B.2.3.
The Fourier transform is a isometric bijection of $\mathcal{S}(\mathbb{R}^d)$ on $\mathcal{S}(\mathbb{R}^d)$ admitting as inverse $\mathcal{F}^{-1}$.

And then, let recall the definition and the main property of the convolution of two functions.

Definition B.2.4. Convolution Product
Let f and g be two functions in $L^1(\mathbb{R})$. For all $x \in \mathbb{R}$:

- $y \longmapsto f(x-y)g(y) \in L^1(\mathbb{R})$
- $y \longmapsto f(y)g(x-y) \in L^1(\mathbb{R})$

The convolution of f with g is defined as:

$$\forall x \in \mathbb{R}, \quad (f*g)(x) = \int_{\mathbb{R}} f(x-y)g(y) \, \mathrm{d}y = \int_{\mathbb{R}} f(y)g(x-y) \, \mathrm{d}y = (g*f)(x)$$

and we have $f*g = g*f \in L^1(\mathbb{R})$.

Property B.2.5.
Let $f, g \in L^1(\mathbb{R})$, by using Fubini's theorem we have:

$$\widetilde{f*g} = \tilde{f}\tilde{g}$$

Let $f, g \in \mathcal{S}(\mathbb{R})$, using Leibniz's formula, we can show that:

$$\forall (\alpha,\beta) \in (\mathbb{N}\times\mathbb{N}), \quad |x^\alpha \partial_x^\beta (fg)|_\infty < \infty \quad i.e. \quad fg \in \mathcal{S}(\mathbb{R}).$$

We now have the fundamental tools to manipulate the Fourier transform.

B.2.2 Existence and uniqueness of solution

We say that $\psi \in C^\infty(\mathbb{R}\times\mathbb{R}_+)$ is uniformly in the Schwartz class if

$$\forall T>0,\ \forall j\in\mathbb{N},\ \forall \alpha,\beta\in\mathbb{N},\qquad \sup_{t\in[0,T]} ||x\mapsto x^\alpha \partial_x^\beta \partial_t^j \psi(x,t)||_\infty < \infty.$$

We will show the following result.

Theorem B.2.6.
For any initial condition $\psi_0\in\mathcal{S}(\mathbb{R}^d)$, there exists a unique function $\psi\in\mathcal{C}^\infty(\mathbb{R}\times\mathbb{R}_+)$, uniformly in $\mathcal{S}(\mathbb{R})$, and is a solution to (55).

Uniqueness of solution

Suppose we have such a solution ψ, by taking $j=0$ we have for all $t\in\mathbb{R}_+$ that $u(\cdot,t)\in\mathcal{S}(\mathbb{R})$. Since the Schwartz space is stable by derivations and included in $L^1(\mathbb{R})$, we can consider the Fourier transform of ψ and its spatial derivative Fourier transform. By choosing $j=1$, it follows that $\partial_t\psi(\cdot,t)$ also belongs to the Schwartz class for all $t\in\mathbb{R}_+$. In this way, we can consider the Fourier transform of (55). The linearity of this operation means that ψ also verifies

$$\begin{cases} \widetilde{\partial_t\psi} - i\widetilde{\partial_{xx}\psi} = 0 & \text{in}\quad \mathbb{R}\times(0,+\infty),\\ \widetilde{\psi(\cdot,0)} = \widetilde{\psi_0} & \text{on}\quad \mathbb{R}. \end{cases} \tag{58}$$

Since $\psi\in C^\infty(\mathbb{R}_+\times\mathbb{R}^d)$ uniformly in the Schwartz class, we can define its partial Fourier transform (in space) $\widetilde{\psi}$ by

$$\begin{aligned} \widetilde{\psi}:\quad & \mathbb{R}\times\mathbb{R}_+\to\mathbb{C}\\ & (\xi,t)\mapsto \widetilde{\psi}(\xi,t) = \widetilde{\psi(\cdot,t)}(\xi). \end{aligned}$$

Lemma B.2.7.
Let $\psi\in\mathcal{C}^\infty(\mathbb{R}\times\mathbb{R}_+)$ be uniformly in the Schwartz class. Then $\widetilde{\psi}\in\mathcal{C}^\infty(\mathbb{R}\times\mathbb{R}_+)$, also $\widetilde{\psi}$ is uniformly in the Schwartz class, and

$$\forall j\in\mathbb{N},\forall t\geq 0,\qquad \partial_t^j\widetilde{\psi}(t,\cdot) = \widetilde{\partial_t^j\psi(t,\cdot)}.$$

Therefore, based on lemma B.2.7 and formula (56), we can state

$$\begin{cases} \partial_t\widetilde{\psi} + i4\pi^2\xi^2\widetilde{\psi} = 0 & \text{in}\quad \mathbb{R}\times(0,+\infty),\\ \widetilde{\psi}(\cdot,0) = \widetilde{\psi_0} & \text{on}\quad \mathbb{R}. \end{cases} \tag{59}$$

By solving the Cauchy problem (59) associated with an ordinary differential equation, for a fixed $\xi\in\mathbb{R}$, we obtain that

$$\forall\xi\in\mathbb{R},\forall t\in\mathbb{R}_+,\quad \widetilde{\psi}(\xi,t) = \widetilde{\psi_0}(\xi)e^{-i4\pi^2\xi^2 t} = \widetilde{\psi_0}(\xi)\mathcal{G}_{i4\pi^2 t}(\xi), \tag{60}$$

where, for all $a\in\mathbb{C}$, we define $\mathcal{G}_a = e^{-a(\cdot)^2}$ the Gaussian kernel. Let's define the set of moderate-growth functions

$$\begin{aligned} \mathcal{O}_M = \{g\in\mathcal{C}^\infty(\mathbb{R},\mathbb{C})/\forall\alpha\in\mathbb{N},\exists C,M\geq 0 \text{ s.t.}\\ \forall x\in\mathbb{R}^d,\ |\partial_x^\alpha g(x)|\leq C(1+|x|^2)^M\}. \end{aligned}$$

It's easy to verify that for all $t>0$, $\mathcal{G}_{i4\pi^2 t}\in\mathcal{O}_M$ and

$$\forall f\in\mathcal{S}(\mathbb{R}),\forall g\in\mathcal{O}_M,\quad fg\in\mathcal{S}(\mathbb{R}). \tag{61}$$

Since $\widetilde{\psi_0}\in\mathcal{S}(\mathbb{R})$ and $\mathcal{G}_{i4\pi^2 t}\in\mathcal{O}_M$, we have for all $t>0$ $\widetilde{\psi}(\cdot,t)\in\mathcal{S}(\mathbb{R})$ and by lemma B.2.3 the uniqueness of $\psi(\cdot,t)$, i.e., the solution:

$$\forall t\in\mathbb{R}_+,\quad \psi(\cdot,t) = \mathcal{F}^{-1}(\widetilde{\psi(t,\cdot)})$$

Existence of solution

After addressing the uniqueness question, we will now demonstrate the existence of a solution to our problem. Let's define

$$\forall t \in \mathbb{R}_+, \quad \phi(\cdot, t) = \mathcal{F}^{-1}(\widetilde{\psi_0}\mathcal{G}_{i4\pi^2 t}).$$

Thus, $\phi(\cdot, t) \in \mathcal{S}(\mathbb{R})$ for all $t \geq 0$, and

$$\forall \xi \in \mathbb{R}, \forall t \in \mathbb{R}_+, \qquad \widetilde{\phi}(\xi, t) = \widetilde{\psi_0}(\xi)\mathcal{G}_{i4\pi^2 t}(\xi).$$

To demonstrate that ϕ is the correct candidate of our problem, we will begin by proving that $\widetilde{\phi} \in C^\infty(\mathbb{R}_+ \times \mathbb{R}^d)$, that $\widetilde{\phi}$ is uniformly in the Schwartz class, and finally $\widetilde{\phi}$ satisfies (58). These findings, with the assistance of lemma B.2.7 (by replacing $\mathcal{F}$ by $\mathcal{F}^{-1}$) and result (56), allow us to assert that ϕ will be the solution to our initial Cauchy problem, that is, $\phi \in \mathcal{C}^\infty(\mathbb{R} \times \mathbb{R}_+)$, uniformly in $\mathcal{S}(\mathbb{R})$, and is a solution to (55). We will show that $\widetilde{\phi}$ is of class C^∞. To do this, we will begin by demonstrating that $(\xi, t) \mapsto \mathcal{G}_{-i4\pi^2 t}(\xi)$ is of class $C^\infty(\mathbb{R} \times \mathbb{R}_+)$. It is known that

$$\begin{aligned} & (\xi, t) \mapsto \xi^2 \in C^\infty(\mathbb{R} \times \mathbb{R}_+), \\ \text{so that} \quad & (\xi, t) \mapsto t\xi^2 \in C^\infty(\mathbb{R} \times \mathbb{R}_+), \\ \text{and} \quad & (\xi, t) \mapsto \exp(-i4\pi^2 t\xi^2) \in C^\infty(\mathbb{R} \times \mathbb{R}_+), \end{aligned}$$

because the composition by the exponential preserves the C^∞ character. Moreover, our assumptions ensure that $\widetilde{\psi_0} \in C^\infty(\mathbb{R})$, so

$$(\xi, t) \mapsto \widetilde{\psi_0}(\xi) \in C^\infty(\mathbb{R} \times \mathbb{R}_+).$$

We deduce that $\widetilde{\phi}$ is the product of functions in $C^\infty(\mathbb{R} \times \mathbb{R}_+)$, consequently $\widetilde{\phi} \in C^\infty(\mathbb{R} \times \mathbb{R}_+)$. We will now show that $\widetilde{\phi}$ is uniformly in the Schwartz class.

Lemma B.2.8.
We define

$$\forall n \in \mathbb{N}, \ \forall \rho \in C^n(\mathbb{R}), \quad p_n(\rho) := \max\left(\{||x \mapsto x^\alpha \partial_x^\beta \rho(x)||_\infty \ \textit{where} \ |\alpha|, |\beta| < n\}\right).$$

A function ρ is in the Schwartz class if and only if for all $n \in \mathbb{N}$ we have $p_n(\rho) < \infty$.

We have that

$$\begin{aligned} \forall j \in \mathbb{N}, \forall \alpha, \beta \in \mathbb{N}, \forall t \in \mathbb{R}_+, \forall \xi \in \mathbb{R}, \quad |\xi^\alpha \partial_\xi^\beta \partial_t^j \widetilde{\phi}(\xi, t)| &= \left| \sum_{\gamma \leq \beta} \binom{\beta}{\gamma} \xi^\alpha \partial_\xi^\gamma \widetilde{\psi_0}(\xi) \partial_\xi^{\beta-\gamma} \left((-i4\pi^2\xi^2)^j \mathcal{G}_{i4\pi^2 t}(\xi)\right) \right| \\ &\leq \sum K |\xi^l \mathcal{G}_{i4\pi^2 t}(\xi) \partial_\xi^\gamma \widetilde{\psi_0}(\xi)| \end{aligned}$$

where the sum is finite, $\gamma \in \mathbb{N}$, $K \in \mathbb{R}$ and $l \in \mathbb{N}$ depend on the summation indices. We have that

$$\forall \gamma \in \mathbb{N}, \forall l \in \mathbb{N}, \forall \xi \in \mathbb{R}, \quad |\xi^l \mathcal{G}_{i4\pi^2 t}(\xi) \partial_\xi^\gamma \widetilde{\psi_0}(\xi)| \leq |\xi^l \partial^\gamma \widetilde{\psi_0}(\xi)| < \infty.$$

The last inequality is performed using that the Schwartz space is stable under differentiation and multiplication by any polynomial. It then can be deduced that

$$\forall T > 0, \ \forall j \in \mathbb{N}, \ \forall \alpha, \beta \in \mathbb{N}, \qquad \sup_{t \in [0,T]} ||\xi \mapsto \xi^\alpha \partial_\xi^\beta \partial_t^j \widetilde{\phi}(\xi, t)||_\infty < \infty,$$

meaning that the function $\widetilde{\phi}$ is uniformly in the Schwartz class. Finally, we have

$$\begin{aligned} & \forall t \in \mathbb{R}_+, \forall \xi \in \mathbb{R}, \quad \partial_t \widetilde{\phi}(\xi, t) = -i4\pi^2 \xi^2 \widetilde{\psi_0}(\xi) \mathcal{G}_{i4\pi^2 t}(\xi) = -i4\pi^2 \xi^2 \widehat{\phi}(\xi, t), \\ \text{and} \ & \forall \xi \in \mathbb{R}, \quad \widehat{\phi}(\xi, 0) = \widetilde{\psi_0}(\xi). \end{aligned}$$

In other words, $\widehat{\phi}$ also satisfies (59). In conclusion, ϕ is the unique function in $\mathcal{C}^\infty(\mathbb{R}_+ \times \mathbb{R}^d)$, uniformly in the Schwartz class, and is a solution of (55). So we've proved the expected result.

B.2.3 Analytical resolution

The objective of this part is to find the expression of u in the spatial and not frequency domain as (60). However, we'll start from this result to determine it but since $\mathcal{G}_{i4\pi^2 t}$ is not in $L_1(\mathbb{R})$, we cannot use the result property B.2.5. The idea is then to extend this result to a space more suitable for our problem. Effectively, therefore the inverse Fourier transform of $\mathcal{G}_{i4\pi^2 t}$ does not exist in the sense of functions, let's try to consider it in the space of distributions, more precisely in the space of tempered distributions. Our plan is therefore as follows: we will start by giving a brief introduction to this space and its properties, then go on to prove the following property

Property B.2.9. *For $T \in \mathcal{S}'(\mathbb{R})$ and $\psi \in \mathcal{S}(\mathbb{R})$,*

$$T * \psi \in \mathcal{S}'(\mathbb{R}) \qquad \text{and} \qquad \mathcal{F}(T * \psi) = \mathcal{F}(T)\mathcal{F}(\psi),$$

which is an extension of property B.2.5 and finally conclude our initial problem.

A reminder of the fundamentals of tempered distributions

We will only briefly review and demonstrate some elements of this theory that we need for our proof. For a more complete analysis, we can refer to chapters 5 and 6 of book [5]. Let recall that the definition of the space of tempered distributions $\mathcal{S}'(\mathbb{R})$.

Definition.

$$\mathcal{S}'(\mathbb{R}) = \left\{ \begin{array}{lll} T \ : & \mathcal{S}(\mathbb{R}) & \to \mathcal{C} \qquad \textit{which is linear and continuous} \\ & \phi & \mapsto \langle T, \phi \rangle \end{array} \right\},$$

considering continuity in the sense of distributions, i.e.,

$$\phi_n \to \phi \ \textit{in}\ \mathcal{S}(\mathbb{R}) \quad \Rightarrow \quad \langle T, \phi_n \rangle \to \langle T, \phi \rangle \ \textit{in}\ \mathcal{C}.$$

In addition, we have the property

Property B.2.10.

$$f \in L^1(\mathbb{R}) \cup L^2(\mathbb{R}) \cup L^\infty(\mathbb{R}) \quad \Rightarrow \quad T_f \in \mathcal{S}'(\mathbb{R}),$$

where T_f is defined such for all $\phi \in \mathcal{S}(\mathbb{R})$, $\langle T_f, \phi \rangle = \int_{\mathbb{R}} f(x)\phi(x)dx$.

In order to define the Fourier transform on this space we have the following theorem

Theorem. *The operator $\mathcal{F}$ from $\mathcal{S}(\mathbb{R})$ to $\mathcal{S}(\mathbb{R})$ has a unique extension to a continuous map of $\mathcal{S}'(\mathbb{R})$ to $\mathcal{S}'(\mathbb{R})$. This operator $\mathcal{F}$ is defined as*

$$\forall T \in \mathcal{S}'(\mathbb{R}), \forall \phi \in \mathcal{S}(\mathbb{R}), \qquad \langle \mathcal{F}T, \phi \rangle = \langle T, \mathcal{F}\phi \rangle$$

It assert that the expression are still meaningful and continuous for function in $\mathcal{S}(\mathbb{R})$.

Indeed, since $\mathcal{F}$ is continuous on $\mathcal{S}(\mathbb{R})$ we have that

$$\langle \mathcal{F}T, \phi_n \rangle = \langle T, \mathcal{F}\phi_n \rangle \to \langle T, \mathcal{F}\phi \rangle = \langle \mathcal{F}T, \phi \rangle.$$

Moreover, we note that the same can be done with the inverse Fourier transform of $\mathcal{S}(\mathbb{R})$ and stay the inverse on $\mathcal{S}'(\mathbb{R})$ since

$$\langle \mathcal{F}^{-1}\mathcal{F}T, \psi \rangle = \langle \mathcal{F}T, \mathcal{F}^{-1}\psi \rangle = \langle T, \mathcal{F}\mathcal{F}^{-1}\psi \rangle = \langle T, \psi \rangle.$$

About Fourier transform and convolution on $\mathcal{S}'(\mathbb{R})$

Let's start by showing that the convolution product between a tempered distribution and a function of $\mathcal{S}(\mathbb{R})$ makes sense in $\mathcal{S}'(\mathbb{R})$. For that we consider $T \in \mathcal{S}'(\mathbb{R})$ and $\psi \in \mathcal{S}(\mathbb{R})$, it comes

$$\begin{aligned} \forall \phi \in \mathcal{S}(\mathbb{R}), \qquad \langle T * \psi, \phi \rangle :&= \int_R (T * \psi)(x)\phi(x)dx \\ &= \int_R \langle T, \phi(x - \cdot) \rangle \phi(x)dx \\ &= \langle T, \int_R \phi(-(\cdot - x))\phi(x)dx \rangle \\ &= \langle T, \psi_\sigma * \phi \rangle, \end{aligned}$$

where $\psi_\sigma(x) = \psi(-x)$. Therefore, since the Schwartz space is stable by convolution, we effectively have that our object $T * \psi$ is well defined on $\mathcal{S}(\mathbb{R})$. Now, thanks to our last theorem, we can consider the Fourier transform of this convolution and write

$$\begin{aligned}\langle \mathcal{F}(T*\psi), \phi\rangle &= \langle T*\psi, \mathcal{F}\phi\rangle \\ &= \langle \mathcal{F}^{-1}\mathcal{F}T, \psi_\sigma * \mathcal{F}\phi\rangle \\ &= \langle \mathcal{F}T, \mathcal{F}^{-1}(\psi_\sigma * \mathcal{F}\phi)\rangle.\end{aligned}$$

But according to property B.2.5 and noting that $\mathcal{F}^{-1}\psi = \mathcal{F}(\psi_\sigma)$ on $\mathcal{S}(\mathbb{R})$, we have

$$\begin{aligned}\mathcal{F}^{-1}(\psi_\sigma * \mathcal{F}\phi) &= \mathcal{F}((\psi_\sigma * \mathcal{F}\phi)_\sigma) \\ &= \mathcal{F}\left(\int_{\mathbb{R}} \psi(-(-\cdot - x))\mathcal{F}\phi(x)dx\right) \\ &= \mathcal{F}\left(\int_{\mathbb{R}} \psi(\cdot + x)\mathcal{F}\phi(x)dx\right) \\ &= \mathcal{F}\left(\int_{\mathbb{R}} \psi(\cdot - x)\mathcal{F}\phi(-x)dx\right) \\ &= \mathcal{F}(\psi * \mathcal{F}^{-1}\phi) \\ &= \mathcal{F}(\psi)\phi.\end{aligned}$$

We deduce the expected result

$$\langle \mathcal{F}(T*\psi), \phi\rangle = \langle \mathcal{F}T, \mathcal{F}(\psi)\phi\rangle = \langle \mathcal{F}T\mathcal{F}(\psi), \phi\rangle.$$

In other word

$$\forall T \in \mathcal{S}'(\mathbb{R}), \forall \psi \in \mathcal{S}(\mathbb{R}), \qquad \mathcal{F}(T*\psi) = \mathcal{F}(T)\mathcal{F}(\psi).$$

We finally proved property B.2.9.

Analytic Gaussian Fourier transform

Let recall our aim here is to compute the inverse Fourier transform of $\mathcal{G}_{4i\pi^2 t}$ (in a first time in the sense of the distributions), so that we can apply property B.2.9 to obtain the spatial expression of our solution of (55).

First, for $a \in \mathcal{C}$ such that $\Re(a) > 0$, $\mathcal{G}_a$ is in $L_\infty(\mathbb{R})$, we can use the property B.2.10 to talk about is associated tempered distribution. Here the idea will to notice that for any $\psi \in \mathcal{S}(\mathbb{R})$, the application $a \mapsto \langle e^{-ax^2}, \psi\rangle$ is holomorphic in $\Re(a) > 0$ and continuous in $\{\Re(a) \geq 0, a \neq 0\}$, then to use to use analytic continuation principle and a p.

Theorem (Analytic continuation principle)**.** *Let U be a convex open of $\mathcal{C}$, and let f and g be two holomorphic functions on U. Let A be a part of U admitting an accumulation point that belongs to U.*
Then,

$$f = g \text{ on } A \quad \Longleftrightarrow \quad f = g \text{ on } U.$$

Remember that for R_+^*, we have

$$\mathcal{F}(x \mapsto e^{-ax^2})(\xi) = (a^{-1}\pi)e^{-\pi^2 a^{-1}\xi^2} \qquad \text{with} \qquad \sqrt{a} = \sqrt{|a|}e^{i\frac{\arg(a)}{2}}.$$

The condition over root of a is equivalent to $\Re(\sqrt{a}) \geq 0$. We therefore have the following equality for R_+^*

$$\langle \mathcal{F}e^{-ax^2}, \psi\rangle = \int_R (a^{-1}\pi)e^{-\pi^2 a^{-1}\xi^2}\psi(x)dx$$

Two sides are holomorphic in $\Re(a) > 0$ and equal on $\Re(a) > 0$, and continuous on $\{\Re(a) \geq 0, a \neq 0\}$. By choosing $U = \Re(a) > 0$ and $A = R_+^*$, the unique continuation principle for analytic functional implies the previous equality on $\Re(a) > 0$. Now by continuity this result can be extended to $\{\Re(a) \geq 0, a \neq 0\}$, i.e., we have proved the following theorem

Theorem B.2.11. *For all $a \in \{\Re(a) \geq 0, a \neq 0\}$,*

$$\mathcal{F}e^{-ax^2} = (a^{-1}\pi)e^{-\pi^2 a^{-1}\xi^2} \qquad \textit{with} \qquad \sqrt{a} = \sqrt{|a|}e^{i\frac{\arg(a)}{2}}.$$

Back to the initial problem

The previous result allow us to write by taking $a = -i\frac{1}{4t}$, which admits as root with positive real part $\sqrt{a} = e^{-i\frac{\pi}{4}}\frac{1}{\sqrt{4t}}$,

$$\begin{aligned} & \mathcal{F}(e^{-i\frac{\pi}{4}}\frac{1}{\sqrt{4\pi t}}e^{i\frac{x^2}{4t}}) = e^{-i4\pi^2 t\xi^2} \\ \Rightarrow \qquad & \mathcal{F}^{-1}(e^{-i4\pi^2 t\xi^2}) = e^{-i\frac{\pi}{4}}\frac{1}{\sqrt{4\pi t}}e^{i\frac{x^2}{4t}} \\ & a = e^{-i\frac{\pi}{4}}\frac{1}{\sqrt{4\pi t}}\mathcal{G}_{-i/4t}. \end{aligned}$$

Now, appealing to property B.2.9, the result (60), the theorem B.2.6 and recalling that $\psi_0 \in \mathcal{S}(\mathbb{R})$, we can conclude in the following theorem.

Theorem B.2.12 (Schrödinger solution)**.**
The unique solution to problem (55) is

$$\forall t \geq 0, \forall x \in \mathbb{R}, \qquad \psi(x,t) = e^{-i\frac{\pi}{4}}\frac{1}{\sqrt{4\pi t}}(\psi_0 * \mathcal{G}_{-i/4t})(x). \tag{62}$$

B.2.4 Application to the example of main article

In accordance with the simulation of [1], let's choose

$$\forall x \in \mathbb{R}, \quad \psi_0(x) = 2\,\mathrm{sech}(\sqrt{2}x)e^{i\frac{15}{2}x}. \tag{63}$$

This is clear that ψ_0 is of class $\mathcal{C}^\infty$, let's now prove that ψ_0 is in the Schwartz class to use what was done before. Since $x \mapsto e^{i\frac{15}{2}x} \in \mathcal{O}_M$, thanks to (61) all that remains is to show that the hyperbolic secant sech is in the Schwartz class. To do this, we begin by showing by recurrence that

$$\forall p \in \mathbb{N},\ \forall x \in \mathbb{R}, \qquad \mathrm{sech}^{(p)}(x) = \frac{P(e^x) + Q(-x)}{(e^x + e^{-x})^{2^p}}, \tag{64}$$

with P and Q are polynomials of degree strictly inferior to 2^p. Since $\mathrm{sech}(x) = 2/(e^x + e^{-x})$, the property is obviously verified at rank 0. We have for all $p \in \mathbb{N}^*$ and for all $x \in \mathbb{R}$,

$$\begin{aligned} \mathrm{sech}^{(p+1)}(x) &= \frac{\partial}{\partial x}\left[\mathrm{sech}^{(p)}\right](x) \\ &= \frac{(P'(e^x) + Q'(e^{-x}))(e^x + e^{-x})^{2^p} - 2p(P(e^x) + Q(e^{-x}))(e^x - e^{-x})(e^x + e^{-x})^{2^p-1}}{(e^x + e^{-x})^{2^{p+1}}} \\ & \qquad \text{with} \quad {}' \equiv \frac{\partial}{\partial e^x}. \end{aligned}$$

Since the set of polynomials is closed by multiplication, we deduce that the numerator can be written as desired (P' and Q' stay polynomial (rk: their degrees don't change)). Now let take interest of their degrees, for that we denote $deg_{e^x}(R)$ (resp. $deg_{e^{-x}}(R)$) the degree of the polynomials R w.r.t e^x (resp. e^{-x}). It thus comes

$$\alpha := deg_{e^x}((P'(e^x) + Q'(e^{-x}))(e^x + e^{-x})^{2^p}) = deg_{e^x}(P'(e^x) + Q'(e^{-x})) + deg_{e^x}((e^x + e^{-x})^{2^p}).$$

We have by definition $deg_{e^x}(P'(e^x) + Q'(e^{-x})) = deg_{e^x}(P'(e^x)) = deg_{e^x}(P(e^x))$, then

$$\alpha = deg_{e^x}(P(e^x)) + 2^p < 2^p + 2^p = 2^{p+1}.$$

by hypothesis. With the same reasoning, it is easy to show that

$$\begin{aligned} deg_{e^{-x}}((P'(e^x) + Q'(e^{-x}))(e^x + e^{-x})^{2^p}) &< 2^{p+1}, \\ deg_{e^x}(2p(P(e^x) + Q(e^{-x}))(e^x - e^{-x})(e^x + e^{-x})^{2^p-1}) &< 2^{p+1}, \\ deg_{e^{-x}}(2p(P(e^x) + Q(e^{-x}))(e^x - e^{-x})(e^x + e^{-x})^{2^p-1}) &< 2^{p+1}. \end{aligned}$$

Then we proved (64), we deduce from that

$$\forall p \in \mathbb{N}, \qquad \operatorname{sech}^{(p)}(x) = \mathcal{O}(e^{-|x|}) \qquad \text{when } x \to \infty,$$

which allow us to write

$$\forall k \in \mathbb{N}, \forall p \in \mathbb{N}, \qquad \lim_{x\to\infty} x^k \operatorname{sech}^{(p)}(x) = 0.$$

We have indeed sech $\in \mathcal{S}(\mathbb{R})$ and therefore verified that $\psi_0 \in \mathcal{S}(\mathbb{R})$. We can now use our theorem B.2.12 to write that the solution of the Schrödinger equation (55) with initial condition (63) is

$$\forall t \geq 0, \forall x \in \mathbb{R}, \qquad \psi(x,t) = e^{-i\frac{\pi}{4}} \frac{1}{\sqrt{4\pi t}} \left(2\operatorname{sech}(\sqrt{2}z) e^{i\frac{15}{2}z} * \mathcal{G}_{-i/4t}(z)\right)(x). \tag{65}$$

C Energy analysis

C.1 Wave equation

Recall the most general form of the 1D wave equation studied here is

$$\partial_{tt}\psi - c^2\partial_{xx}\psi = c^2 Q, \tag{66}$$

for a positive (or null) source term Q. Multiplying by $\frac{\partial\psi}{\partial t}$ and integrating over spatial domain :

$$\begin{aligned}
0 &= \int_\Omega \frac{\partial^2\psi}{\partial t^2}\frac{\partial\psi}{\partial t}dx - c^2\int_\Omega \frac{\partial^2\psi}{\partial x^2}\frac{\partial\psi}{\partial t}dx - c^2\int_\Omega Q(x,t)\frac{\partial\psi}{\partial t}dx \\
&= \frac{1}{2}\frac{d}{dt}\int_\Omega \left|\frac{\partial\psi}{\partial t}\right|^2 dx - c^2\int_\Omega \frac{\partial^2\psi}{\partial x^2}\frac{\partial\psi}{\partial t}dx - c^2\int_\Omega Q(x,t)\frac{\partial\psi}{\partial t}dx \qquad \text{using } \frac{\partial^2\psi}{\partial t^2}\frac{\partial\psi}{\partial t} = \frac{1}{2}\frac{\partial}{\partial t}\left((\frac{\partial\psi}{\partial t})^2\right) \\
&= \frac{1}{2}\frac{d}{dt}\int_\Omega \left|\frac{\partial\psi}{\partial t}\right|^2 dx + c^2\frac{1}{2}\frac{d}{dt}\int_\Omega \left|\frac{\partial\psi}{\partial x}\right|^2 dx - c^2\int_\Omega Q(x,t)\frac{\partial\psi}{\partial t}dx \quad \text{using an IBP, then } \frac{\partial^2\psi}{\partial t\partial x}\frac{\partial\psi}{\partial x} = \frac{1}{2}\frac{\partial}{\partial t}\left((\frac{\partial\psi}{\partial x})^2\right)
\end{aligned}$$

Here, we periodic boundary condition in space to make boundary terms in the integration by parts (IBP) vanish. From here, one can define the total energy as :

$$E(t) = \frac{1}{2}\int_\Omega \left[\left|\frac{\partial\psi}{\partial t}\right|^2 + c^2\left|\frac{\partial\psi}{\partial x}\right|^2\right]dx,$$

where the term containing time derivative corresponds to kinetic energy and the one with space derivative to potential energy. Integrating the last line of computation over time $[0,T]$ gives :

$$E(t) = E(0) + c^2\int_0^T\int_\Omega Q(x,t)\frac{\partial\psi}{\partial t}(x,t)dxdt. \tag{67}$$

One can see that if there is no source term ($Q\equiv 0$) then the total energy remains constant over time, which is desirable. However, for non zero Q, the total energy increases over time, which is logical as if energy is injected into the (spatial) domain, then the total energy changes. Note that Q could be negative to model an energy sink.

C.2 Schrödinger equation

Recall that for problem eq. (55) with $\psi_0(\mathbb{R}) \in \mathcal{S}(\mathbb{R})$, we proved in appendix B.2.3 that the analytical solution ψ verifies (60), that is,

$$\forall\xi\in\mathbb{R}, \forall t\in\mathbb{R}_+, \quad \widetilde{\psi}(\xi,t) = \widetilde{\psi_0}(\xi)\mathcal{G}_{i4\pi^2 t}(\xi).$$

Theorem (Plancherel theorem)**.** *The Plancherel theorem ensures that for $f\in L^2(\mathbb{R})$,*

$$||f||_2 = ||\widetilde{f}||_2.$$

Thanks to theorem B.2.6, we can ensure that $\psi\in\mathcal{S}(\mathbb{R})\subset L^2(\mathbb{R})$, therefore for all $t\geq 0$ we have

$$||\psi(\cdot,t)||_2 = ||\widetilde{\psi}(\xi,t)||_2 = ||\widetilde{\psi_0}\mathcal{G}_{i4\pi^2 t}||_2.$$

Since $\mathcal{G}_{i4\pi^2 t}$ is initial we have

$$||\psi(\cdot,t)||_2 = ||\widetilde{\psi_0}||_2,$$

i.e., the norm of the solution is effectively independent of time. Moreover, by applying Plancherel's theorem once again, we have

$$\forall t\in\mathbb{R}^+, \qquad ||\psi(\cdot,t)||_2 = ||\psi_0||_2.$$

D Convergence of the schemes

In the framework of linear equation, the convergence of a scheme is guaranteed as soon as the scheme has proven to be consistent and stable. Consistency concerns the fact that the scheme is indeed a good approximation to the equation, meaning that for a time and space step tending to 0, the approximation tends to the exact solution (assuming it exists). Stability denotes the behaviour of a scheme to have bounded error. In our case, we use Von Neumann stability analysis which looks at ratios of Fourier terms of the Fourier series expansion of the approximation, making sure they do not blow up in high frequencies. As before, we will denote ψ the exact solution to a given problem, $\psi|_j^n = \psi(j\Delta x, n\Delta t)$ and finally ψ_j^n its approximation.

D.1 Wave equation

First recall that the wave equation we use if formulated as :

$$\partial_t \psi - c^2 \partial_{xx} \psi = 0 \tag{68}$$

where c is real and denotes the velocity. We use an explicit finite difference scheme to compute solutions to this equation, given by

$$\frac{\psi_j^{n+1} - 2\psi_j^n + \psi_j^{n-1}}{\Delta t^2} = c^2 \frac{\psi_{j+1}^n - 2\psi_j^n + \psi_{j-1}^n}{\Delta x^2} \tag{69}$$

Consistency analysis

Assuming the solution to the wave equation is twice differentiable in time and space, we can use Taylor-Lagrange expansions of ψ to get :

$$\begin{cases} \dfrac{\psi|_j^{n+1} - 2\psi|_j^n + \psi|_j^{n-1}}{\Delta t^2} - \partial_{tt}\psi|_j^n = \frac{\Delta t^2}{12}\partial_{4t}\psi|_j^n + o(\Delta t^2) \\ \dfrac{\psi|_{j+1}^n - 2\psi|_j^n + \psi|_{j-1}^n}{\Delta x^2} - \partial_{xx}\psi|_j^n = \frac{\Delta x^2}{12}\partial_{4x}\psi|_j^n + o(\Delta x^2) \end{cases} \tag{70}$$

Assembling those relations to approximate time and space derivative in the original equation provides the full scheme :

$$\frac{\psi|_j^{n+1} - 2\psi|_j^n + \psi|_j^{n-1}}{\Delta t^2} = c^2 \frac{\psi|_{j+1}^n - 2\psi|_j^n + \psi|_{j-1}^n}{\Delta x^2} \tag{71}$$

This scheme is thus consistent of order 2 in time and space. In fact, when Δx and Δt tend to 0, the approximation error does so.

Stability analysis

We will use the Von Neumann analysis framework. To do this, we identify $\psi_j^n \longleftrightarrow \Gamma^n e^{ipj\Delta x}$ for Γ, p some real numbers corresponding to some frequency p in the Fourier domain and its associated modulus Γ. The aim is to restrict $|\Gamma| < 1$. Injecting this identification in the scheme, we get

$$\Gamma^2 - 2\Gamma + 1 = C\Gamma(-4\sin^2(p\Delta x)) \quad \Longleftrightarrow \quad \Gamma^2 - 2\left[2 + 2C(\cos(p\Delta x) - 1)\right]\Gamma + 1 = 0 \tag{72}$$

where $C = c^2\frac{\Delta t^2}{\Delta x^2}$ the CFL number. In what follows, we denote $B = 2 + 2C(\cos(p\Delta x) - 1)$. First remark that this is a second order polynomial equation which unknown is Γ. It can be solved with the use of the discriminant, which is $\Delta = B^2 - 4$.

- If $\Delta > 0$, then $B^2 > 4$. However, we see that B can not be bigger than 2, which means that for such value for the discriminant to be reached, one has $B < -2$. The discriminant being positive, the equation admits two real roots :

  $$\Gamma_\pm = \frac{B \pm \sqrt{B^2 - 4}}{2}$$

  However, one can observe that $\Gamma_- < \frac{B}{2} < \frac{-2}{2} = -1$, which means instability. Thus, this condition on the discriminant does not enable to find criterion to restrict the modulus of Γ.

- If $\Delta \leq 0$, then we have $-2 \leq B \leq 2$ and two complex roots

$$\Gamma_{pm} = \frac{B \pm i\sqrt{4 - B^2}}{2}.$$

As one can check, this provides stability for sure as $|\Gamma_\pm| = \Gamma_+\Gamma_- = 1$. It lasts to find what is the restriction imposed on C by this case.

$$-2 \leq 2 + 2C(\cos(p\Delta x) - 1) \leq 2$$
$$-2 \leq C(\cos(p\Delta x) - 1) \leq 0$$

The right inequation is always satisfied as the cos function is always smaller than 1. However, the left hand-side has to be checked. In the worst case of $\cos(p\Delta x) \approx 1$, we get that $C \leq 1$, which is the CFL condition for the scheme.

Thanks to Von Neumann stability analysis, we derived a criterion to ensure that the error does not blow up during the simulation, which is that $c\frac{\Delta t}{\Delta x} \leq 1$.

Conclusion

We have seen that the scheme is consistent, meaning that increasing the mesh resolution induces a reduction of the approximation error. Moreover, we have derived a stability criterion. If those two conditions are satisfied, then one can be sure that the scheme converged towards the strong solution of the wave equation.

D.2 Schrödinger equation

First recall the equation that is approximated, considering a null potential, on the interior of the domain

$$\partial_t \psi - i\partial_{xx}\psi = 0 \tag{73}$$

and recall the Crank-Nicolson scheme that is used to approximate the problem at the interior of the domain

$$\frac{\psi_j^{n+1} - \psi_j^n}{\Delta t} = \frac{i}{2(\Delta x)^2}\left[\left(\psi_{j+1}^{n+1} - 2\psi_j^{n+1} + \psi_{j-1}^{n+1}\right) + \left(\psi_{j+1}^{n} - 2\psi_j^{n} + \psi_{j-1}^{n}\right)\right]. \tag{74}$$

Consistency analysis

Assuming the solution to the Schrödinger equation is twice differentiable in time and four times differentiable in space, we can write the following Taylor-Lagrange expansion of ψ :

$$\begin{cases} \dfrac{\psi|_j^{n+1} - \psi|_j^n}{\Delta t} - \partial_t\psi|_j^n = \dfrac{\Delta t}{2}\,\partial_{tt}\psi|_j^n + o(\Delta t) & \text{(75a)} \\ \dfrac{\psi|_{j+1}^{n} - 2\psi|_j^{n} + \psi|_{j-1}^{n}}{\Delta x^2} - \partial_{xx}\psi|_j^n = \dfrac{\Delta x^2}{12}\partial_{4x}\psi|_j^n + o(\Delta x^2) & \text{(75b)} \\ \dfrac{\psi|_{j+1}^{n+1} - 2\psi|_j^{n+1} + \psi|_{j-1}^{n+1}}{\Delta x^2} - \partial_{xx}\psi|_j^{n+1} = \dfrac{\Delta x^2}{12}\partial_{4x}\psi|_j^{n+1} + o(\Delta x^2) & \text{(75c)} \end{cases}$$

Then, performing the linear combination (75a)$-\frac{i}{2}$[(75b)+(75c)] provides the error term when the scheme is applied to a true solution of the equation. Note that $\partial_{tt}\psi = -\partial_{4x}\psi$. Denoting τ_j^n the FD scheme applied to ψ in the left member of the linear combination (75a)$-\frac{i}{2}$[(75b)+(75c)] we get

$$\tau_j^n - \left[\partial_t\psi|_j^n - \frac{i}{2}\left(\partial_{xx}\psi|_j^n + \partial_{xx}\psi|_j^{n+1}\right)\right] = -\frac{\Delta t}{2}\,\partial_{4x}\psi|_j^n + i\frac{\Delta x^2}{24}\left(\partial_{4x}\psi|_j^n + \partial_{4x}\psi|_j^{n+1}\right) + o(\Delta t, \Delta x^2). \tag{76}$$

To get to the equivalent PDE, we need to retrieve equation (73) in the brackets of the left member. For this we use the following relation:

$$\partial_t\psi|_j^n - \frac{i}{2}\left(\partial_{xx}\psi|_j^n + \partial_{xx}\psi|_j^{n+1}\right) = \partial_t\psi|_j^n - i\partial_{xx}\psi|_j^n + \frac{i}{2}\left(\partial_{xx}\psi|_j^n - \partial_{xx}\psi|_j^{n+1}\right).$$

But $\partial_{xx}\psi|_j^n - \partial_{xx}\psi|_j^{n+1} = -\Delta t\partial_{3x}\psi|_j^n + o(\Delta t)$, leading to the equivalent PDE :

$$\frac{\psi|_j^{n+1} - \psi|_j^n}{\Delta t} - i\frac{\left[\left(\psi|_{j+1}^{n+1} - 2\psi|_j^{n+1} + \psi|_{j-1}^{n+1}\right) + \left(\psi|_{j+1}^n - 2\psi|_j^n + \psi|_{j-1}^n\right)\right]}{2(\Delta x)^2} - \left[\partial_t\psi|_j^n - i\partial_{xx}\psi|_j^n\right]$$
$$= -\frac{\Delta t}{2}\left(i\partial_{3x}\psi|_j^n + \partial_{4x}\psi|_j^n\right) - i\frac{\Delta x^2}{24}\left(\partial_{4x}\psi|_j^n + \partial_{4x}\psi|_j^{n+1}\right) + o(\Delta t, \Delta x^2) \tag{77}$$

This provides a way to show what error is made with the Crank-Nicolson scheme for homogeneous Schrödinger equation. In fact, one can see that both dispersion and dissipation are induced by the truncation as some third and fourth order spatial derivatives appear; it also proves the scheme is consistent of order 1 in time and 2 in space. In fact, if Δt and Δx tend to 0, the error vanishes, meaning the approximation with this scheme is consistent.

Stability

Before proving any stability condition for this scheme, we will prove a lemma to help up reduce the computations for the stability proof.

Lemma D.2.1. *Let $\alpha \in \mathbb{R}$, then for any $z \in \mathbb{C}$ such that $\frac{z-1}{z+1} = \alpha i$, one gets $|z| = 1$.*

Proof. Let $\alpha \in \mathbb{R}$, and$z \in \mathbb{C}$ such that $\frac{z-1}{z+1} = \alpha i$. Then one has $z = \frac{1+\alpha i}{1-\alpha i} = \frac{1-\alpha^2}{1+\alpha^2} + i\frac{2\alpha}{1+\alpha^2}$. Thus $|z|^2 = \left(\frac{1-\alpha^2}{1+\alpha^2}\right)^2 + \left(\frac{2\alpha}{1+\alpha^2}\right)^2 = \frac{1-2\alpha^2+\alpha^4+4\alpha^2}{(1+\alpha^2)^2} = \frac{(1+\alpha^2)^2}{(1+\alpha^2)^2} = 1.$ □

Using Von Neumann analysis, we identify $\psi_j^n \longleftrightarrow \Gamma^n e^{ipj\Delta x}$ for Γ, p some real numbers corresponding to some frequency p in the Fourier domain and its associated modulus Γ. Injecting this in the scheme provides:

$$\frac{\Gamma - 1}{\Delta t} = \frac{i}{2\left(\Delta x\right)^2}\left[\Gamma\left(e^{ip\Delta x} - 2 + e^{-ip\Delta x}\right) + \left(e^{ip\Delta x} - 2 + e^{-ip\Delta x}\right)\right]$$

leading, using that $\left(e^{ip\Delta x} - 2 + e^{-ip\Delta x}\right) = (2i)^2\sin^2(p\frac{\Delta x}{2})$, to the equality :

$$\frac{\Gamma - 1}{\Gamma + 1} = i\frac{\Delta t}{2\Delta x}(-4)\sin^2(p\frac{\Delta x}{2})$$

which by lemma D.2.1 gives that $|\Gamma| = 1$ so that Von Neumann stability criterion is always satisfied, i.e., the scheme is unconditionally stable.

Conclusion The Crank-Nicolson scheme being consistent and stable for the Schrödinger equation, which admits a solution, the scheme converges to this solution.

References

[1] X. Antoine, E. Lorin, and Q. Tanga. "A Friendly Review of Absorbing Boundary Conditions and Perfectly Matched Layers for Classical and Relativistic Quantum Waves Equations". In: (Oct. 2017). DOI: 10.1080/00268976.2017.1290834.

[2] X. Antoine and C. Besse. "Unconditionally stable discretization schemes of non-reflecting boundary conditions for the one-dimensional Schrödinger equation". In: *Journal of Computational Physics* 188.1 (2003), pp. 157–175. ISSN: 0021-9991. DOI: https://doi.org/10.1016/S0021-9991(03)00159-1. URL: https://www.sciencedirect.com/science/article/pii/S0021999103001591.

[3] Lawrence C. Evans. *Partial Differential Equations*. Jan. 1988. DOI: 10.1007/bfb0082920.

[4] Jean-Pierre Bony. *Cours d'analyse: théorie des distributions et analyse de Fourier*. fr. Editions Ecole Polytechnique, 2001. ISBN: 978-2730207751.

[5] Elliott H. Lieb and Michael Loss. *Analysis*. American Mathematical Society (AMS), 2001. ISBN: 978-0-8218-2783-3.